Helena Anzjøn

Mercury in Marine Arctic Sediments

Master's thesis in MLREAL
Supervisor: Murat V. Ardelan
Co-supervisor: Nicolas Sanchez

May 2022

Master's thesis

NTNU
Norwegian University of Science and Technology
Faculty of Natural Sciences
Department of Chemistry

NTNU
Norwegian University of
Science and Technology

Helena Anzjøn

Mercury in Marine Arctic Sediments

Master's thesis in MLREAL
Supervisor: Murat V. Ardelan
Co-supervisor: Nicolas Sanchez
May 2022

Norwegian University of Science and Technology
Faculty of Natural Sciences
Department of Chemistry

NTNU
Kunnskap for en bedre verden

Abstract

Increasing temperatures due to climate change are expected to release mercury stored in permafrost and accelerate the export of mercury from Siberian rivers into the Arctic Ocean (Liem-Nguyen *et al.*, 2022; Schuster *et al.*, 2018). To study the potential Hg input from permafrost thawing the total mercury (THg) concentration has been determined from 60 surface sediment samples taken from the Kara Sea, the Laptev Sea, and the East Siberian Sea, and ten core sediment samples from the Kara Sea. The sampling of the core sediments took place in October 2021, and the sampling of the surface sediments were conducted in October 2020.

A Direct Mercury Analyser (DMA-80) was used to analyse THg. Concentrations of THg from the surface sediments ranged from 1,99 ng/g to 70,52 ng/g, and the average for the Kara Sea, The Laptev Sea, and the East Siberian Sea were 35,56 ng/g, 35,28 ng/g, and 48,28 ng/g, respectively. The mercury concentration in the sediment cores ranged from 11,60 ng/g to 76,79 ng/g. These samples show a general tendency of decreasing concentrations with increasing sediment depth (Figure 4.2), and seven of the ten cores show higher concentration in the surface layer than in the deepest sediment interval. There is no clear evidence for permafrost being the source of mercury in the sediments, but the results support the need for further research on permafrost thawing releasing mercury.

Sammendrag

Økende temperaturer grunnet klimaendringer forventes å frigjøre kvikksølv lagret i permafrost, og øke mengden kvikksølv som blir transportert til Arktiske hav fra elver i Sibir (Liem-Nguyen *et al.*, 2022; Schuster *et al.*, 2018). For å studere potensielt kvikksølv input fra permafrost tining har den totale kvikksølv (THg) konsentrasjonen blitt analysert og bestemt fra 60 overflate sediment prøver fra Kara havet, Laptev havet, og det Øst Sibirske hav, og i tillegg har ti prøver av kjernesedimenter fra Kara havet blitt analysert. Prøvetakingen fra kjerneprøvene ble utført i oktober 2021, og overflate prøvene ble tatt i oktober 2020.

En "Direct Mercury Analyser" (DMA-80) ble brukt for å utføre analyser av THg. THg konsentrasjonen i prøvene av overflate sediment varierte fra 1,99 ng/g til 70,52 ng/g, og gjennomsnittet for Kara havet, Laptev havet og det Øst Sibirske hav var henholdsvis 35,56 ng/g, 35,28 ng/g, og 48,28 ng/g. THg konsentrasjonen i prøvene av kjernesediment varierte fra 11,60 ng/g til 76,79 ng/g. Disse prøvene viser en generell trend med synkende konsentrasjon med økende dybde i sedimentene (Figur 4.2), og syv av ti sediment kjerneprøver har høyere konsentrasjon i sediment overflaten enn i det dypeste intervallet. Det er ingen klare bevis for at tining av permafrost er kilden til kvikksølv i sedimentene, men resultatene underbygger behovet for videre studier på kvikksølv i Arktiske sedimenter og tining av permafrost.

Acknowledgements

This thesis was carried out as a part of the MLREAL program at the department of chemistry. Working with this thesis has given me valuable insight in scientific methodology and has given me a deeper understanding of environmental chemistry, which I will find useful in my future career in teaching chemistry and science.

I want to thank my supervisor Murat Ardelan for sharing his enthusiasm for this project and giving me invaluable insight. In addition, I would like to thank my co-supervisor, Nicolas Sanches, who was always available for questions and guidance. Furthermore, I am grateful to and want to thank Kyyas Seyitmuhammedov and Stephen Kohler for their technical support on the freeze dryer, the DMA-80 instrument, and the ODV-software. I also want to thank Alicia Garcia and Christina Segovia Martin for helping analyse and prepare the samples from 2020. And, lastly, I want to thank Monica Breivik, my lunch buddy and motivational force.

Table of content

List of Figures

List of Tables

1 Introduction

Mercury is hazardous to the natural environment and poses a risk to human health. Methylmercury (MeHg) is toxic and bioaccumulates through the food chain. Human populations in the Arctic have elevated MeHg levels compared to other parts of the world, and it has been raised concern about elevated amounts of mercury in the Arctic. (AMAP, 2021; Calder, Bromage and Sunderland, 2019; Soerensen *et al.*, 2016).

The Arctic is among the most sensitive regions to climate change, and air temperatures have risen more than twice the rates seen elsewhere (AMAP, 2021; Overland *et al.*, 2019). Warmer temperatures are thawing permafrost, melting glaciers, and eroding coastlines, which impact the biogeochemical cycle of mercury. Permafrost stores approximately twice as much mercury as all other soils, the ocean, and the atmosphere combined (Schuster *et al.*, 2018). It is estimated that the soil in the permafrost regions contains 1656 ± 962 Gg Hg in the top three meters of soil, of which 793 ± 461 Gg Hg are frozen in permafrost (Schuster *et al.*, 2018). If greenhouse emissions continue at their current rate, a $30 - 99\%$ reduction in permafrost areas in the Northern Hemisphere is predicted (Koven, Riley and Stern, 2013). Thus, increasing the release of mercury into the Arctic Ocean through river outlets.

This thesis aims to investigate if permafrost thawing will contribute to elevated levels of mercury in Arctic sediments. It seeks to provide an overview of the current levels of mercury in Arctic sediments and explain the sources of mercury emissions into Arctic oceans. This is done by analysing sediment samples from 2020 and 2021 with a Direct Mercury Analyser (DMA-80) instrument. The total mercury concentration (THg) is compared with location, depth of the water column, and earlier studies from the same area. This is used to observe an understand the distribution of mercury in Arctic sediments. The samples are taken from the Kara Sea, the Laptev Sea, and the East Siberian Sea and include 60 different sampling locations, where 10 of these sampling stations have sediment cores. The sampling of sediments is part of a larger project called BEST-Siberian, which aims to provide data and knowledge on the environmental and ecological risks due to increasing mobility and transformation of bio-essential and toxic trace elements, such as mercury, on the Siberian continental shelf under permafrost thawing (NFR, 2021). The overall purpose of this thesis is to contribute to new knowledge concerning mercury in marine Arctic sediments.

2 Background

2.1 Mercury (Hg)

Mercury has the atomic number 80 in the periodic table, it has high vapor pressure but is still heavy and dense, and it is the only metal that is liquid at room temperature (Britannica, 2021). The unique properties of mercury have made it an attractive element for human use. It has been used in thermometers, to make amalgams with silver for fillings in dentistry, and to extract gold and silver from mining (Britannica, 2021). Mercury is still in use today; for example in batteries, electric switches, fluorescent tubes, flat-screen monitors, and pharmaceuticals (Decharat, 2018; WHO, 2017). The awareness of mercury's toxicity has led to a replacement of the metal in many areas, but anthropogenic activities like coal mining still release Hg into the environment (Beckers and Rinklebe, 2017).

The primary natural emission sources of Hg into the atmosphere and environment are volcanic emissions, weathering, and forest fires (Li and Tse, 2015). Anthropogenic sources include the burning and combustion of fossil fuels, coal mining, and industries such as ore and cement production (Chen *et al.*, 2014). In addition, unregulated electronic waste (e-waste) leads to mercury being released into the environment (Baldé *et al.*, 2020; Decharat, 2018; Galappaththi and Suraweera, 2020). It is estimated that globally 50 tons of mercury exist in undocumented e-waste annually, which is largely released into the environment (Baldé *et al.*, 2020). The anthropogenic sources make up two-thirds of the total Hg emissions and contribute to a disturbance in the Hg-cycle. Elemental mercury (Hg^0) is both volatile and stable in the atmosphere (0,5-2 years) and its distribution depends on the air-circulation (Li and Tse, 2015). Mercury can therefore be spread over large areas of the atmosphere, to places with no local emission source and is considered a global pollutant (Beckers and Rinklebe, 2017; WHO, 2017).

Mercury has no known biological function and is considered a non-essential element (Meador, Ernest and Kagley, 2005). However, studies indicate that some bacteria take up mercury actively, raising questions about its cellular function (Morel, 2016; Schaefer *et al.*, 2011). Mercury is hazardous to the natural environment and poses a risk to human health. Inhaled elemental mercury will accumulate in the red blood cells and be transported to different tissue in the body (Li and Tse, 2015). Long-term exposure could lead to defects in the nervous, digestive, and immune systems (WHO, 2017). The mobility and toxicity of the metal are dependent on its speciation (Beckers and Rinklebe, 2017).

An international effort to reduce mercury emissions and ban mercury-mining was made through the "Minamata Convention on mercury", which derives its name from one of the best-known examples of mercury being released directly into the nearby marine environments in the town of Minamata (Beckers and Rinklebe, 2017; UNEP, 2013). Hg-contaminated waste was released for

thirty years from a local acetaldehyde factory, which resulted in a vast amount of MeHg that bioaccumulated in fish and was consumed by Minamata's inhabitants (UNEP, 2013). This caused many habitants to develop severe damage to their nervous system and gave a name to the "Minamata disease" caused by mercury poisoning (UNEP, 2013). The first patient with this disease was reported in January 1956, and by 2011 a total of 2273 victims had been officially recognized as having Minamata disease (Yorifuji, Tsuda and Harada, 2013). Of the first 1422 patients reported to have Minamata disease, 378 had died by the end of 1980 (Tamashiro *et al.*, 1984). The Minamata convention aims "to protect the human health and the environment from anthropogenic emissions and releases of Hg and Hg compounds" by phasing out existing mercury mines and banning new ones, as well as monitoring emissions of Hg and reducing the use of Hg in products and in industy(Beckers and Rinklebe, 2017). The convention was agreed upon in 2013, and it entered into force in 2017. It currently has 128 signatories and 137 parties (Beckers and Rinklebe, 2017). The current general focus on health impacts caused by mercury focuses on chronic, low, or moderate exposures (Ye *et al.*, 2016).

2.1.1 Mercury Speciation and Environmental Compartments

Mercury has three oxidation states: 0 (elemental mercury), I (monovalent mercury), and II (divalent mercury). Oxidation states 0 and II are the two main oxidation states as monovalent mercury is not stable under environmental conditions (Beckers and Rinklebe, 2017). Both Hg (I) and Hg (II) form several inorganic and organic chemical compounds. In the environment, mercury is found within three major species: elemental mercury (Hg^0), inorganic divalent mercury (Hg (II)/ Hg^{2+}), and organic mercury (mostly MeHg) being methyl mercury (MeHg) the most common form (Li and Tse, 2015). MeHg has no industrial uses and occurs naturally where environmental conditions favour the methylation of mercury (Beckers and Rinklebe, 2017). Methylation of Hg is a process that is primarily biologically mediated by anaerobic bacteria, but can also though abiotic mechanisms (Hsu-Kim *et al.*, 2013). MeHg is generally more toxic than other organic mercury compounds (Li and Tse, 2015). One exception is dimethylmercury (DMeHg), a volatile and extremely toxic compound, where even small amounts adsorbed through human skin can be fatal (West *et al.*, 2020). DMeHg is volatile and unstable, and is thought to play a role in the amount of Hg accumulated in food chains as it can act as a source for MeHg when it is demethylated (Lian *et al.*, 2021; West *et al.*, 2020).

Hg^{2+} is the oxidized form of mercury and exists naturally in the environment in divalent cationic salts with mercury, for example, with sulphur (HgS) or chloride ($HgCl_2$) (Li and Tse, 2015). Hg^{2+} is the most water-soluble form of mercury and will deposit from the atmosphere quicker than Hg^0 (Beckers and Rinklebe, 2017). (Beckers and Rinklebe, 2017). As elemental mercury is oxidized by chloride to Hg^{2+} in the ocean, there is a higher concentration of Hg^{2+} in the ocean than Hg^0. Hg^{2+} is more bioavailable than elemental mercury and can accumulate in the liver and kidneys of humans (Li and Tse, 2015). Due to soil and sediments properties for redox potential

and pH and strong Hg-sorbents, Hg^{2+} is the most abundant form in this environmental compartment (Beckers and Rinklebe, 2017).

MeHg represents 1% of the total Hg in sediments, and 10-30% of the total Hg in water, whereas it represents 80% of the total amount of mercury in fish (Li and Tse, 2015). MeHg bioaccumulates, and less than 10% of Hg in the human body can be excreted and thus removed (Li and Tse, 2015). The same is true for fish, which leads to the biomagnification of mercury through the food chain, meaning that the concentration of Hg in a predator is higher than for its prey. The toxicity of MeHg is higher than it is for inorganic mercury, and it is known to block sites of enzymes and interfere with protein synthesis (Li and Tse, 2015; Maggi *et al.*, 2009). Humans are readily exposed to MeHg through seafood and rice consumption.

2.1.2 Sources of Emission and Transport of Hg

Mercury is released to the environment through natural and anthropogenic sources. Once it has entered the environment, Hg cycles between the major environmental compartments air, soil, and water until removed through burial in deep ocean sediments and mineral soils (UNEP, 2013). Figure 2.1 shows a simplification of the Hg-cycle. Hg emissions are usually categorised into three sources: natural, anthropogenic, and re-emissions of already-deposited Hg that initially had a natural or anthropogenic source (UNEP, 2013). Emissions can also be divided into primary and secondary sources, where primary sources of Hg can be both natural and anthropogenic. Primary sources transfer mercury from long-lived lithospheric reservoirs to the atmosphere, which then deposits on land and in oceans (Driscoll *et al.*, 2013). Primary sources increase the total amount of Hg in surface reservoirs, while secondary sources represent the re-emissions and redistributed Hg within ecosystems (Driscoll *et al.*, 2013).

The natural sources of Hg emission are mainly volcanic eruptions and weathering of rocks, which are assumed to be constant except for changes in volcanic activity. It was estimated in 2013 that the annual release of Hg into the air from natural sources was around 80 – 600 t/y (UNEP, 2013). Other estimations on the annual emission from both natural sources and re-emission range between 3600 – 5300 t/y (Sundseth *et al.*, 2017). However, it has been pointed out that it is difficult to distinguish between natural and anthropogenic emissions and re-emissions as different measures use different models, and estimations given vary by as much as 100% (Gworek *et al.*, 2017).

It is however still clear that human activities have disrupted the Hg-cycle and increased Hg-emissions (AMAP, 2011; Amos *et al.*, 2013; Sunderland and Mason, 2007; UNEP, 2013). Sunderland and Mason (2007) concluded that anthropogenic activity has resulted in about three times as much mercury being emitted into the atmosphere than was before the industrial revolution. The total mercury emissions were estimated to be 20% higher in 2015 than in 2010,

and emissions have continue to raise in recent years (AMAP, 2021). The primary anthropogenic sources constitute 30% of the total global emissions, while the primary natural sources are estimated to make up about 10% (AMAP, 2021). The remainder is from the secondary re-emissions. Most of the re-emissions originate from anthropogenic sources, and reducing new anthropogenic sources is a major factor in reducing mercury build-up in the environment (AMAP, 2021). However, as Amos et al. (2013) pointed out, reducing new anthropogenic sources will not reduce the amount of mercury deposited and accumulating into ecosystems. If the anthropogenic sources are kept constant in the future, the Hg deposition in the environment will still increase due to mercury accumulating in the biogeochemical cycle (Amos *et al.*, 2013).

Atmospheric transport of mercury plays a significant role in the Hg-cycle due to the long residence time of Hg^0 and its ability to be transported by wind currents (Li and Tse, 2015). Mercury is unique compared to other trace metals in the atmosphere because the majority of it is present as gaseous elemental mercury (GEM), whereas other metals are primarily associated in the atmosphere with aerosols (Skov *et al.*, 2006). The main form of mercury transported through the atmosphere is elemental and inorganic (AMAP, 2021). The transport of Hg within the atmosphere is rapid compared with other environmental reservoirs, and the time scale for global mixing in the troposphere is about one year, mainly limited by air exchange between the two hemispheres (Driscoll *et al.*, 2013). This indicates that Hg can be transported all over the world. However, as the mixing of air between the hemispheres is a limiting factor, around 30% higher concentrations of total gaseous Hg in the northern than in the southern hemisphere have been observed (Driscoll *et al.*, 2013). Air from the northern hemisphere travels and mixes with the air in the Arctic, and some of these airmasses are then returned after cycling through the Arctic (Douglas *et al.*, 2012).

Atmospheric Hg can be deposited into aquatic systems or terrestrial environments, and its fate depends on its speciation and environmental conditions. Mercury has a strong affinity to organic matter, which affect its mobility (Beckers and Rinklebe, 2017). Rivers discharge 28 ± 13 Mmol/y of mercury into the ocean margins globally, while atmospheric deposition account for 10 – 29 Mmol/y (Zhang *et al.*, 2015). Most of the riverine mercury is buried in the ocean margin sediment through particle settling, but approximately 6% is transported globally to the open ocean (Zhang *et al.*, 2015). The main vector for the transport of terrestrial Hg through riverine systems is organic carbon (Liem-Nguyen *et al.*, 2022). In soils, mercury is generally bound to solids, and only a small fraction is found in the aqueous phase (O'Connor *et al.*, 2019). The speciation of mercury in soils is usually mercuric salts or minerals. The mercuric salt's solubility varies widely, and so does its potential to be transported (O'Connor *et al.*, 2019). The release of mercury from soils is thought to be mainly from the volatilization of elemental mercury, and discharge from soil to groundwater is considered negligible (Beckers and Rinklebe, 2017). Coastal erosion mobilizes mercury bound in the soil and transfers it into the ocean (Dastoor *et al.*, 2022). Mercury in the soil can also be taken up into roots due to its strong binding capacity to organic ligands, and this mercury is mainly not transported with the movement of water through

the plant (Mason, 2009). Several estimates of the average total Hg concentration in the world's soils have been made. The lower estimations are between 0.01-0.06 ppm, and the higher estimations are between 0.58-1.8 ppm (Beckers and Rinklebe, 2017). Beckers and Rinklebe (2017) state that the mining of mercury for the past five centuries along with the coal burning and ore industry during the last decades, have caused a major release of mercury into the atmosphere and consequently soil uncontaminated by mercury pollution cannot be found.
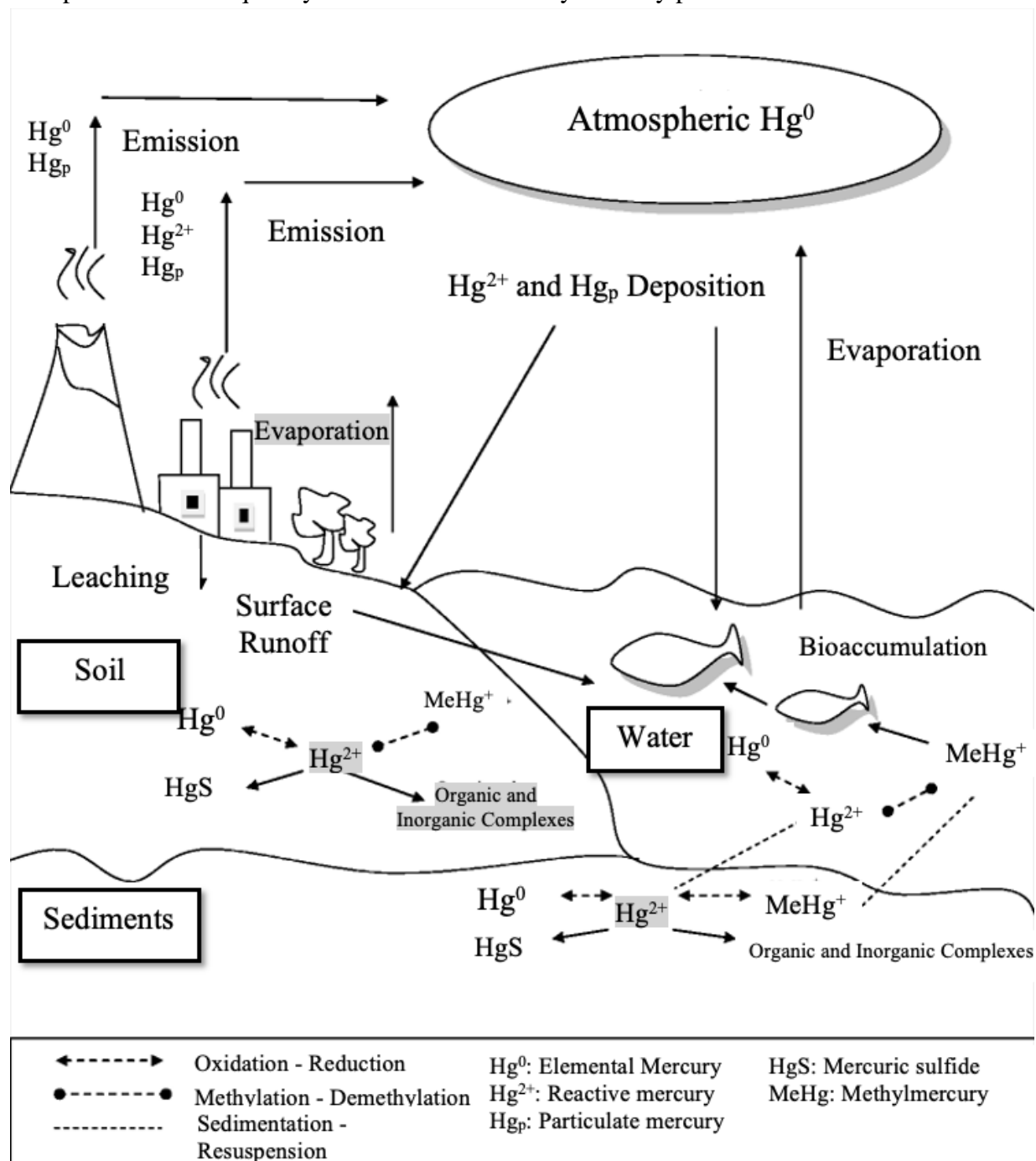
Figure 2.1: A simplified overview of the biogeochemical cycle of mercury in the environment (Li and Tse, 2015).

2.2 Mercury in the Arctic

The Arctic and its exceptional seasonality ranging from 24 hours of darkness in the winter to 24 hours of sunlight during the summer, greatly affect the Arctic's Hg-cycle, which also exhibits exceptional seasonality (Douglas *et al.*, 2012). The Arctic Ocean makes up around 1% of the world's oceans by volume, but receives 11% of the global runoff, which is enhanced due to the seasonality (McClelland *et al.*, 2012). In addition, a significant amount of the runoff comes from locations under permafrost that is thawing due to climate change (Douglas *et al.*, 2012; McClelland *et al.*, 2012). The high amount of runoff into the Arctic Ocean as well as the melting and freezing of ice, leads to the upper part, approximately 0 – 50 meters of it, being stratified and limits the deeper part of the ocean in exchanging components with the atmosphere. The stratification varies with the seasons as more runoff is received during the summer, thus enhancing stratification (Douglas *et al.*, 2012). A consequence of this is that the deep sea of the Arctic Ocean has lower particulate export, and bio-active elements, including Hg, tend to recycle in the upper stratified layer (Douglas *et al.*, 2012). In the winter season, weak stratification will promote downward transport of particles together with strong mixing (Olli *et al.*, 2002).

The Arctic is among the most sensitive regions to climate change, and air temperatures have risen more than twice the rates seen elsewhere (AMAP, 2021; Overland *et al.*, 2019). This is due to feedback mechanisms that include a reduction in sea ice as the sea is melting, allowing the surface of the sea to absorb more solar radiation, which in turn leads to increasing temperatures and more melting of sea ice (Douglas *et al.*, 2012). This will affect how mercury moves through the Arctic ecosystem. Warmer temperatures are thawing permafrost, melting glaciers, and eroding coastlines, which impact the biogeochemical cycle of mercury. A simplified model of mercury cycling in the Arctic is shown in Figure 2.2.

Mercury is transported to the Arctic by the atmosphere, ocean, and rivers and adds to the Hg-cycle in Artic water, soils, sediments, ice, plants, and animals (AMAP, 2021; Dastoor *et al.*, 2022). In the Arctic, episodic depletion of Hg^0 from the atmosphere is observed regularly during the polar sunrise in the spring (Carignan and Sonke, 2010). This is due to oxidation by halogen radicals, mainly bromine, being released photochemically from sea salt deposited on snow ice (Ferrari *et al.*, 2008; Fisher *et al.*, 2013). A correlation has been found between decreasing gaseous elemental mercury (GEM) in the atmosphere and an increasing concentration of divalent mercury in snow and soil (Skov *et al.*, 2006). This is due to atmospheric mercury depletion events (AMDEs), which contribute to an increase in Hg deposition (AMAP, 2011; Fisher *et al.*, 2013). Studies have shown that after each AMDE, about 80% of the deposited Hg on the snow-surface will be re-emitted as GEM back into the atmosphere (AMAP, 2011). The bioavailable fraction of the newly deposited mercury has been shown to be deposited in snowfall events in a higher proportion than deposition provoked by AMDEs (Douglas *et al.*, 2012).

The seasonal melting of sea ice and glaciers plays a major role in the mercury cycle in the Arctic. Melting is estimated to release 0,4 Mg/y of deposited Hg stored in glaciers, which is exported by glacial rivers into the ocean (Dastoor *et al.*, 2022). Uptake and transport of mercury in sea ice is determined by the ice's thickness and permeability, which varies with the seasons. The cold winter makes the ice less permeable and slows the transport of mercury through the ice. In the spring the ice is more permeable, leading to dissolved mercury being released from the ice into the underlying water, and particle-bound mercury and MeHg being incorporated into the sea ice (Wang, Pućko and Stern, 2017). The dynamic motion of sea ice makes it possible to transfer mercury over time and space as the ice can drift over large areas in the Arctic Ocean, depending on winds and currents. One of the two main routes of sea-ice drift in the Arctic is via the Transpolar Drift (TPD) that circulates from the eastern to the central Arctic. The other main route is the Beaufort cycle which circulates clockwise in the eastern Arctic (Agather *et al.*, 2019). TPD is a current that transports river-influenced shelf water from the Laptev and East Siberian Seas toward the centre of the basin, making it possible for trace elements to journey from river outlets (Charette *et al.*, 2020). The TPD has elevated levels of total mercury concentrations and no elevated MeHg (Agather *et al.*, 2019; Charette *et al.*, 2020).

Mercury related consequences of climate change include: alterations in mercury transport from terrestrial areas, changes in the rate at which bacteria convert mercury to methylmercury, and the thawing of permafrost, which stores nearly twice as much Hg as all other soils (AMAP, 2021; Dastoor *et al.*, 2022; Schuster *et al.*, 2018; Soerensen *et al.*, 2016). In addition, a warmer climate will cause a spread of vegetation (also known as Arctic greening) that may increase the amount of atmospheric mercury accumulated in plants and soils. However, it is difficult to understand precisely how each isolated factor will contribute to changes in the Hg-cycle, as the various drivers are complex and interact with each other. In addition, the climatic changes related impacts are uneven across the Arctic, further complicating our understanding of the impacts of climate change (AMAP, 2021).

It has been found that biomagnification of MeHg is higher in cold and low-productivity regions due to higher productivity leading to a "dilution" of MeHg, and so lower amounts are transferred up the food chain (Wu *et al.*, 2021). Inuit people living in the Arctic are one of the most exposed humans to methylmercury worldwide, and human populations in the Arctic have elevated MeHg levels compared to other parts of the world (AMAP, 2021; Calder, Bromage and Sunderland, 2019; Soerensen *et al.*, 2016). This is a result of a diet consisting mainly of seafood with species high up in the food chain that have elevated MeHg levels compared to lower latitudes (Dastoor *et al.*, 2022; Kim, H. *et al.*, 2020).
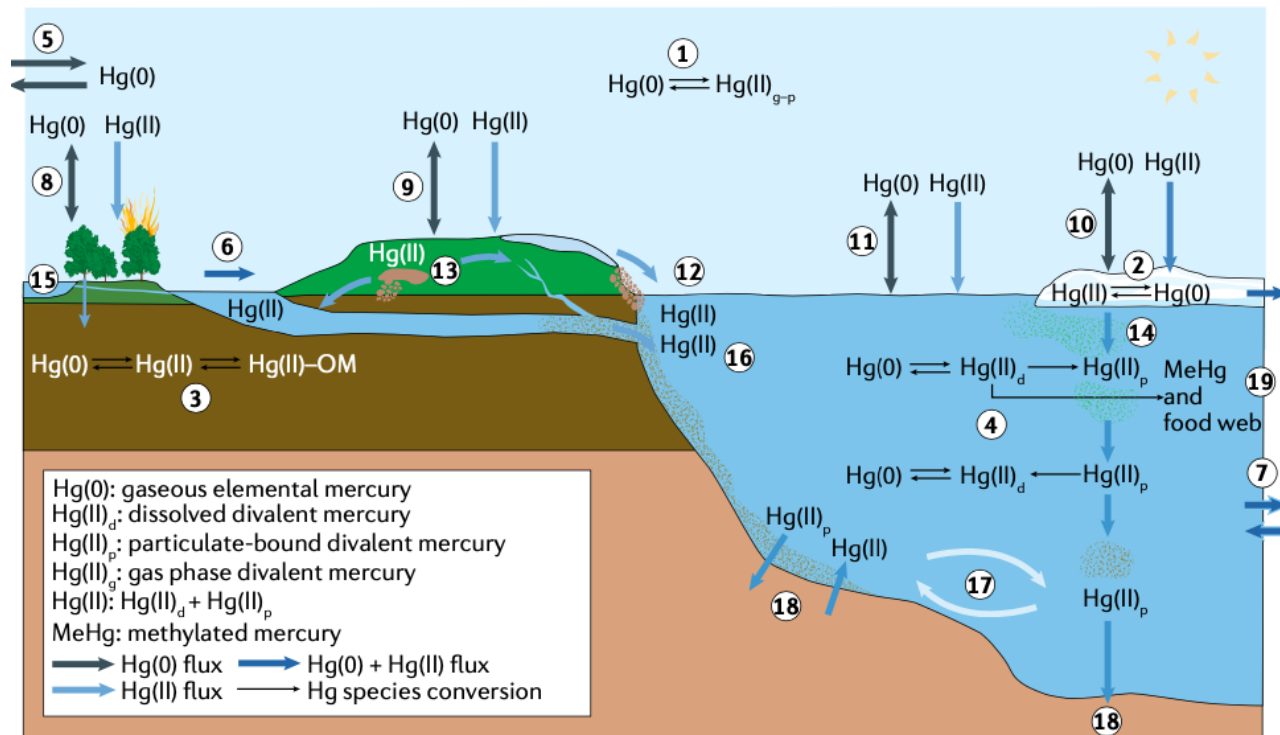
Figure 2.2: Describes the cycling of mercury in the Arctic. The numbers represent different processes. Hg is transported to the Arctic through air (5), rivers (6), and ocean currents (7). Hg stored in terrestrial reservoirs is mobilised through ice melting (14), permafrost thaw (12), soil erosion (13), weathering, and surface runoff (13). Process 17 and 18 show how Hg in the Arctic Ocean is distributed by currents and settles, and process 19 shows the biological uptake and release of Hg. (Dastoor *et al.*, 2022)

2.3 Permafrost Thawing

Permafrost is defined as soil, bedrock, and earth material where the temperature has not exceeded 0 °C for two consecutive years (Lilleøren, 2021). Once the earths material freezes, microbial decay ceases and locks the chemical components into the frozen permafrost (Schaefer *et al.*, 2020). Due to climate change and global warming, the permafrost in the northern regions has begun to thaw and is vulnerable to further thawing (Chadburn *et al.*, 2017; Meredith *et al.*, 2019; Schuster *et al.*, 2018). An estimation made in 2013, based on anthropogenic greenhouse emissions continuing at the current rate, predicts that in 2100 we could have a 30-99% reduction of the Northern Hemisphere permafrost area (Koven, Riley and Stern, 2013). The surface soil layer that lies on top of the permafrost is referred to as "the active layer". This layer thaws in the summer and freezes in the winter and could be increasing in thickness due to increasing temperatures (Meredith *et al.*, 2019). Permafrost thawing could lead to the release of vast amounts of greenhouse gaseous as well as introducing more dissolved organic carbon and particulate organic carbon to the water column (AMAP, 2021; Schuur *et al.*, 2015). Therefore, the permafrost thawing could contribute to even further global warming.

Through deposition from the atmosphere, large amounts of mercury have been stored in permafrost soils for several thousands of years (Schaefer *et al.*, 2020). An estimation made by Schuster et al. (2018) is that "soils in the permafrost regions contain 1656 ± 962 Gg Hg in the top three meters of soil, of which 793 ± 461 Gg Hg are frozen in permafrost" (Schuster *et al.*, 2018). Permafrost stores approximately twice as much mercury as all other soils, the ocean, and the atmosphere combined (Schuster *et al.*, 2018). Another estimation is that 7% of the global soil Hg pool is contained in the upper 30 cm of permafrost (Lim *et al.*, 2020). This indicates that permafrost thawing will also contribute to an increase in released mercury through the discharge of mercury by rivers into the Arctic (Aksentov *et al.*, 2021). It has been shown that there is an increased export of particulate mercury into Siberian rivers in areas surrounded by permafrost compared to areas with no permafrost (Lim *et al.*, 2019). The released mercury has the potential to bioaccumulate and cause damage to the aquatic ecosystem (Meredith *et al.*, 2019)

According to Schaefer et al. (2020), Hg has four release pathways from the terrestrial biosphere: evasion from microbial decay, leaf stomata transpiration, fire, and leaching into groundwater. They further pointed out that most of the liberated Hg from microbial decay is reabsorbed by plants and soil (Schaefer *et al.*, 2020). When permafrost thaws, microbial decay will consume organic matter and release Hg. Schuster et al. (2018) estimated that the turnover time associated with microbial decay for frozen organic matter is around 14 000 years. However, considering the estimated reduction of the permafrost, the turnover time will drop to around 70 years (Schuster *et al.*, 2018), making this a critical and worrying situation.

2.4 Mercury in Sediments

The analysis of marine sediments constitutes an important monitoring tool for aquatic environments, providing information on the accumulation of pollutants (ISO, 2004). If the conditions are ideal, sediment can be deposited in chronological order so that the changes in deposition can be related to a certain period of time (ISO, 2004). Pollutants such as heavy metals bind with particles as they settle through the water column and are incorporated into sediments (Manahan, 2017). For pollutants from sediment core analysis to give a time record for pollution, the sediment analysed must be undisturbed, and the rate of sedimentation should be estimated (Hogarh *et al.*, 2016). Sedimentation rate refers to the amount of material deposited over time, and it will impact the accuracy of core-analysis. The sedimentation rate depends on the distance to the source of particulate matter, the amount of material being introduced, and the preservation and accumulation of particles (Libes, 2011). The usual method of calculating the sedimentation rate is based on the contents and measurement of ^{210}Pb (Aksentov *et al.*, 2021; Rusakov, Borisov and Solovieva, 2019). Gobeil *et al.* (1999) states that sediments from the deep ocean are poor locations to evaluate modern contaminant trends due to slow sedimentation rates compared to sediments in the coastal region (Gobeil, Macdonald and Smith, 1999). However, some studies point to the mercury accumulation in deep oceans being higher than previously thought (Sanei *et*

al., 2021; Liem-Nguyen *et al.*, 2022). In the Arctic Ocean sediments, the Hg concentrations have been found to be higher in the deep basin (60.4 ± 44.5 ng/g) compared to the shelf sediments (28.9 ± 22.0 ng/g) (Dastoor *et al.*, 2022). Rusakov *et al*. (2019) states that waves and sea currents in terrigenous shallow marine sediments do not allow thin clay particles to accumulate in the bottom sediment, and therefore have a lower sedimentation rate than sediment in the deep open sea.

In general, sediments are considered sinks for pollutants and reduce their harm to the environment. However, mercury could be an exception, due to its ability to be mobilized by methylation from anoxic bacteria in oxygen-deficient sediments (Manahan, 2017). An increasing amount of mercury in sediments could make mercury more bioavailable than before it was deposited. Marine sediments exchange mercury with overlying seawater through sedimentation, resuspension, and diffusion of Hg species (Dastoor *et al.*, 2022). The vertical distribution of trace elements in sediments are affected by diageneses processes. Diagenesis processes start with aerobic oxidation of organic matter by using dissolved oxygen from the overlying water. When the oxygen is consumed, the decomposition of organic matter can occur by using NO_3^-, Manganese or Iron hydroxides, and SO_4^{2-} (El Houssainy *et al.*, 2020). However, this order can be disturbed due to the presence of microenvironments with conditions controlled by different bacterial populations (El Houssainy *et al.*, 2020).

Overall, knowledge on the accumulation of mercury in sediments is limited (Sanei *et al.*, 2021). However, the burial rate of mercury is estimated to be 3.9 ± 0.7 Mg/y in the deep basin, and 20 ± 14 Mg/y in shelf sediments (Dastoor *et al.*, 2022). It is believed that particle organic matter (POM) scavenging, and sedimentation of mercury from the euphotic zone is the main source of mercury in deep-ocean sediments, and that the source of mercury in the euphotic zone is mainly from atmospheric deposition (Sanei *et al.*, 2021). Sanei *et al.* (2021) provide two other possible sources that contribute to high mercury concentrations in deep ocean sediments: Firstly, the redistribution of mercury could result from the decomposition of POM containing mercury and thus releasing it into the porewater. Secondly, a high concentration of mercury in deep oceans could be due to hydrothermal vents (Sanei *et al.*, 2021). Globally hydrothermal vents are thought to contribute little to the amount of mercury in oceans, but it could be important locally (Sanei *et al.*, 2021). Another hypothesis about how mercury is transported out in the open ocean in arctic areas is that sedimentary material is brought with glacier meltwaters and is transported to the water surface without being deposited and then transferred to the open sea (Rusakov, Borisov and Solovieva, 2019).

The amount of mercury in sediments will vary with location and sediment conditions, such as particle size and the amount of organic carbon present. Studies have found that sediments with a high mercury concentration have a high supply of organic carbon (Aksentov *et al.*, 2021; Liu *et al.*, 2019). Conversely, sediments consisting of coarse particles have less affinity for trace

elements such as lead and mercury (Budko *et al.*, 2022; Liu *et al.*, 2019). In general, the finer the sediment is, the higher the trace element concentration will be due to the increase in specific surface area of clay minerals (Cauwet, 1987). Cauwet (1987) points out that it is difficult to correct for grain size distribution of sediment samples when analysing trace elements and will only be useful when analysing samples from the same homogenous area.

2.4.1 Recommended Limits of Hg Exposure

Several exposure limits of mercury have been established, meaning that a concentration above the given limit will negatively impact human health or the surrounding environment and its organisms. These limits have been set to determine when mercury levels are concerning. For instance, a Norwegian system for classifying the environmental quality of marine sediments exists (Bakke *et al.*, 2010). The classification is based on the toxicity of the contaminants and the European Union's systems for defining environmental quality standards and performing risk assessments. The aim is to establish a common tool to describe environmental conditions. The system has five concentration intervals, where each class limit represents expected increasing damage to the surrounding environment and its organisms (Miljødirektoratet, 2020). The limits are based on available information from research on risk assessments and ecotoxicological data (Miljødirektoratet, 2020). Figure 2.3 describes the classification classes, and Figure 2.4 show mercury's limit values in Norway.

The majority of the concentration limits that have been set for mercury are suggested for seafood (Ye *et al.*, 2016). To establish if mercury levels in sediments are worrisome for humans, it is necessary to know how much mercury will enter the food chain. Considering how Inuit people in the arctic have some of the highest methylmercury levels worldwide due to a diet consisting of seafood, it could be said that the current limits of mercury in the Arctic are too high.

I Background	II Good	III Moderate	IV Bad	V Very bad
Background levels	No toxic effects	Toxic effects following chronic exposure	Toxic effects following short term exposure	Severe acute toxic effects

Figure 2.3: The principles of the Norwegian quality classification system of contaminants in seawater and sediments (Bakke *et al.*, 2010; Miljødirektoratet, 2020).

Element	Unit	I Background	II Good	III Moderate	IV Bad	V Very bad
Hg	(ng/g)	0 - 50	50 - 520	520 - 750	750 – 1450	> 1450

Figure 2.4: Class limit values for mercury (Miljødirektoratet, 2020)

2.5 Instrumentation – Direct Mercury Analyser

Direct Mercury Analyser (DMA 80) is an instrument that measures the total mercury content, both inorganic and organic, in soil, sediments, and aqueous solutions without sample chemical pre-treatment (EPA., 1998). It is equally suitable for solid and liquid samples and has an instrument detection limit of 0,01 ng (EPA., 1998; Maggi *et al.*, 2009). The typical working range of the instrument is 0,05 – 600 ng (EPA., 1998). The instrument integrates the thermal decomposition sample preparation and atomic absorption detection, which reduces the time needed for analysis (EPA., 1998). This operating principle eliminates most matrix effects and allows the measurement of solid samples with calibration with liquid phase standards (Gueu, Ouffoué and Digbéhi, 2021). If mercury is bound to silicates or other matrices that cannot be thermally decomposed the DMA 80 analysis should be validated and confirmed using a different method (EPA., 1998). Figure 2.5 gives a simplified overlook of the instrument.

The following is a description of the DMA80-analysing procedure described in the EPA 7473 (EPA., 1998). The sample is put into boats that consist of either quartz or nickel. The sample boat is automatically introduced to a quartz decomposition tube heated by two different and independently programmable furnaces: the decomposition and the catalyst furnace. Both furnaces can hold a temperature of at least 750 °C. The sample is dried and then thermally decomposed in an oxygen environment which releases mercury vapor. The decomposition products are carried by a flow of oxygen to the catalytic section of the furnace. Here oxidation is completed, and halogens, nitrogen and sulphur oxides are trapped. The remaining decomposition products are then transported to a gold amalgamator selectively trapping mercury. The purpose of the amalgamator is for mercury to form metal alloys with gold, thereby trapping the mercury. Oxygen is then flushed through the system to remove any residue of gases or decomposition products, and the amalgamator is heated rapidly to 700 °C, which then desorbs and releases mercury vapor. The oxygen flow then carries this vapor through two absorption cuvettes in series. The mercury vapor is first carried through a long pathlength absorbance cell followed by a shorter pathlength absorbance cell with the ratio of 10:1. The same mercury quantity is measured twice with two different sensitivities. The flow path through the spectrometer and cuvettes remained at 120°C to prevent condensation and minimize carry-over effects. Quantification is done by measuring absorbance at 253,7 nm as a function of mercury concentration, and the detector is connected to a computer. (EPA., 1998; Maggi *et al.*, 2009)
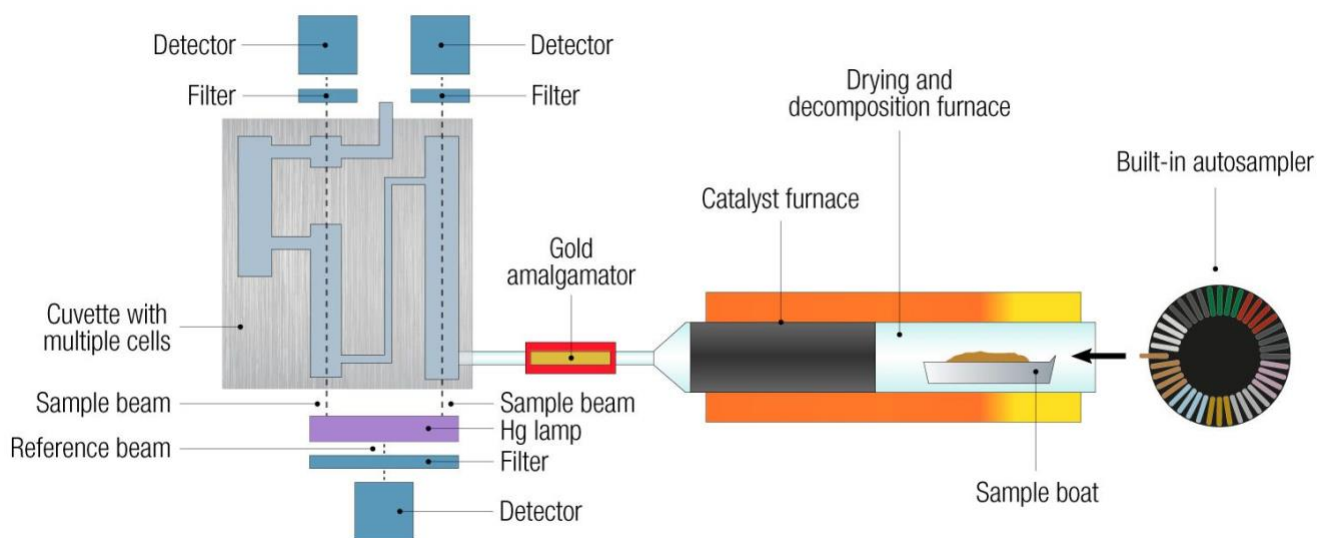
Figure 2.5: Representation of the DMA-80 instrument (Milestone-Srl, 2022).

2.6 Quality Assurance and Quality Control

When working with environmental samples, it is preferable to have as much control as possible during each step of the procedure, and the effects that each step could have on the sample. These steps include sampling, transportation, storage, sample preparation, identification, and quantification, all of which represents potential sources of contamination (Batley, 1999). To ensure that the experimental data presented are of an acceptable standard and give a good indication of the true result, several measures must be made to assure that the results are accurate, precise, and reliable. These measures constitute quality assurance (QA) and quality control (QC) (Fifield and Haines, 2000). QA is an overall procedure ensuring that the analytical operation follows the quality standards, including development, validation, and monitoring. QC is more of a planned system of activities designed to assess the precision and accuracy of an assay and the stability of the samples (Crosby and Prichard, 1995).

Important factors for the QA are matrix effects, calibrations standards, and reference material (Fifield and Haines, 2000). Matrix effects include changes the sample matrix could make to how the analyte is conducted in the result. It is difficult to fully allow for matrix effects in calibration standards unless the matrix is very simple (Fifield and Haines, 2000). Analysis of validated standards known as certified reference material (CRM) is essential in checking the method's performance, and these are accepted both nationally and internationally (Fifield and Haines, 2000). The reference material should have a similar composition to the sample in terms of matrix and concentration (Fifield and Haines, 2000). This will ensure the accuracy of the method.

14

Quality controls are used to ensure precision in the method. Precision refers to the repeatability and reproducibility of the method. Reproducibility refers to variations in the result due to changing conditions, while repeatability refers to variation in repeated measurements made under identical conditions (Crosby and Prichard, 1995). To ensure reproducibility blanks, duplicates, and spiked control samples are important features for ensuring a good result (EPA., 1998). There are several ways to use blanks for quality control, method blanks involve taking a blank sample through the sample-preparation procedures, it should contain all sample components except the analyte. A field blank can be distilled water and is brought out and exposed to the same conditions as the samples taken in the field, and a reagent blank is a blank that is similar to the method blank but is not taken through the sample preparation steps (Batley, 1999; EPA., 1998).

For sediment sampling, it is essential that the equipment does not contaminate the sample. When the target analytes are heavy metals, the samples should be transferred to plastic containers to ensure that the container does not contaminate the samples (ISO, 2004).

The sensitivity of the method should be established and is defined as "the smallest change in analyte concentration that can be reliably detected using the test method" (Crosby and Prichard, 1995). Meaning that the ratio of change in the instrument's response and analyte concentration is measured as the slope of the calibration curve. The limit of detection (LOD) and limit of quantification (LOQ) is often used with sensitivity (Crosby and Prichard, 1995; MacDougall and Crummett, 1980). The LOD is the lowest concentration of an analyte that the analytical process can detect and is often defined as three times the standard deviation of the blank samples, while the lower and upper LOQ are the lowest and highest concentrations, respectively, of an analyte that the analytical process can reliably detect. LLOQ is often defined as ten times the standards deviation of the blank (Batley, 1999).

3 Materials and methods

3.1 Study Area and Sampling

The samples analysed are part of a larger project called BEST-Siberian. BEST-Siberian aims to provide data and knowledge of the environmental and ecological risks due to increasing mobility and transformation of bio-essential and toxic trace elements, such as mercury, on the Siberian continental shelf under permafrost thawing (NFR, 2021). The samples analysed are from two different oceanographic cruises, conducted in October 2020 and 2021 with the research vessel "Akademik Mstislav Keldysh". For the 2020 cruise, surface sediment samples were collected in three different regions: 31 samples taken from the Laptev Sea, 10 samples from the East-Siberian Sea, and 8 samples from the Kara Sea. The samples collected from the 2021 cruise corresponded to multi-core samples, including 47 samples from 11 different stations, all taken from the Kara Sea. The exact location of each station is given in Table A.1 in Appendix A. Maps of the sampling locations are shown in Figures 3.1 to 3.5.

The sampling stations are spread over a large area north of Siberia, Russia. All the stations lie within the arctic environment, and the terrestrial land enclosing the different seas all have permafrost. The sampling region is highly impacted by coastal and subsea permafrost degradation (Shakhova *et al.*, 2017; Overduin *et al.*, 2007). The Kara Sea, the Laptev Sea, and the East-Siberian Sea are all marginal seas of the Arctic and have sea-temperatures below 0 °C in the winter (Britannica, 2014; 2012). The seas start freezing in October or November and thaw around June-July, and all of them have inflow from rivers and ice thawing in the summer (Britannica, 2014; 2012). The Laptev Sea is the outlet for the Lena River, which has the largest annual Hg flux (6600 kg/y) of all Arctic Rivers (Zolkos *et al.*, 2020). This is also the shallowest sea in the Arctic, with an average depth of 48 m (Liem-Nguyen *et al.*, 2022). Other great rivers are the Ob River and the Yenisei River, which flow out into the Kara Sea, and the Kolyma River, which has its outlet into the East Siberian Sea. The Arctic shelf is controlled by Siberian river discharge, ice formation and melting, and exchange with the Arctic Ocean and adjoining seas (Dmitrenko *et al.*, 2010). The Eastern Siberian shelf is the shallowest shelf region of the entire Arctic Ocean with an average depth of 20 – 30 m (Dmitrenko *et al.*, 2010). In the last decade, there has been substantial growth in destination shipping between the Artic and ports outside the region, meaning that the sampling area has experienced an increase in shuttle traffic from ships (Aksentov *et al.*, 2021; Gunnarsson and Moe, 2021).
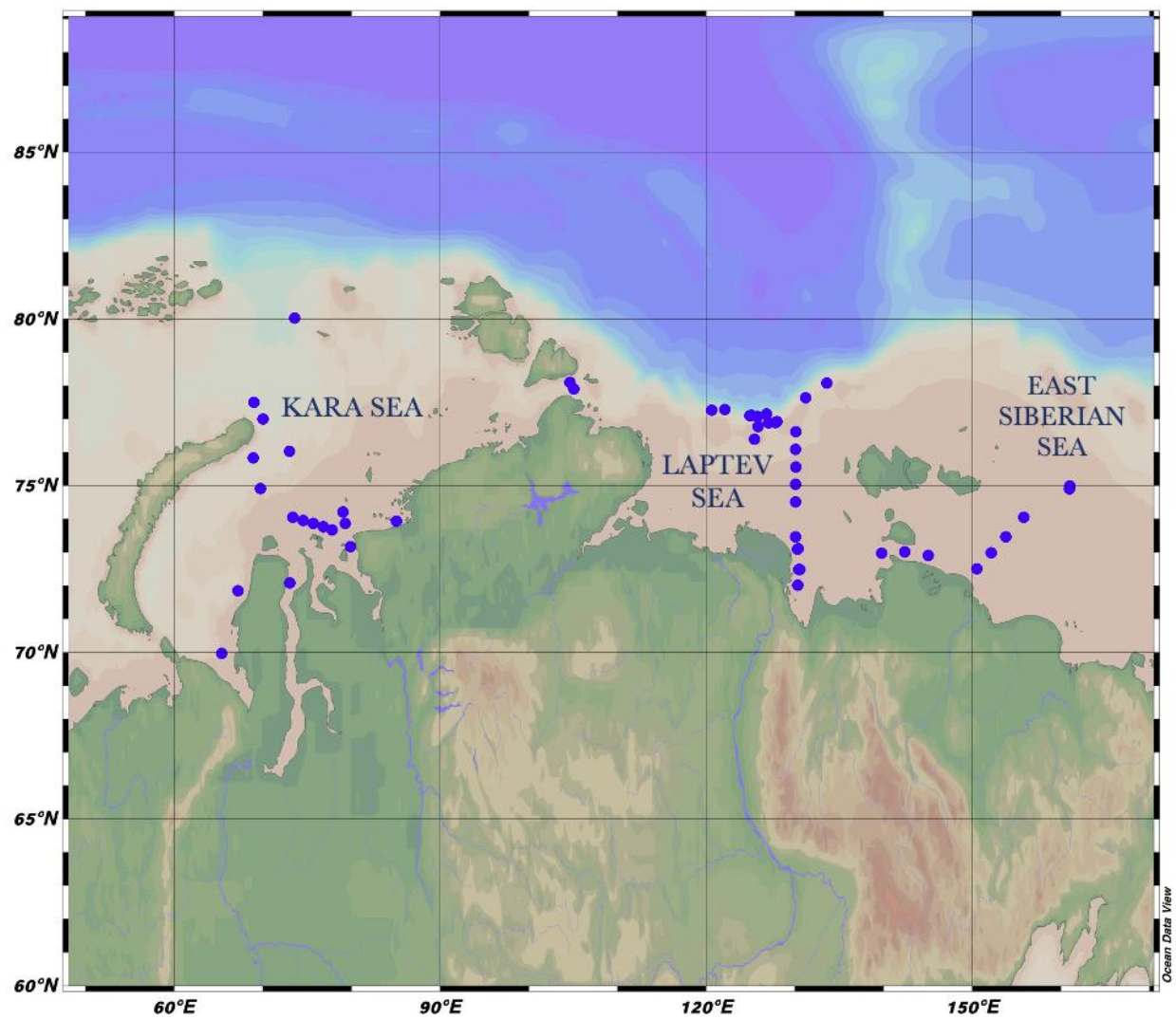
Figure 3.1: Map of all sample locations
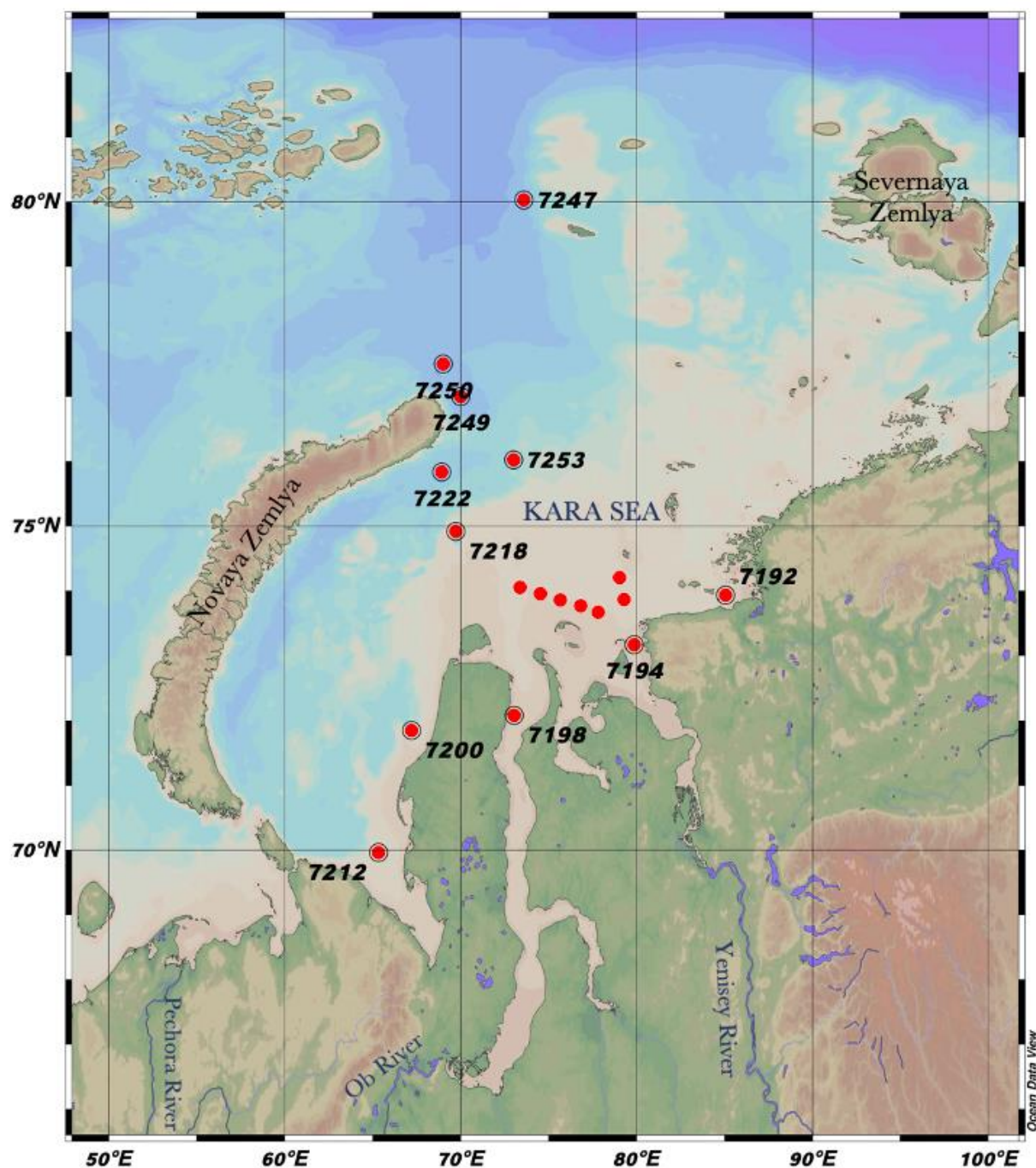
Figure 3.2: A mapping of sample stations in the Kara Sea. The numbered stations represent samples taken in 2021.
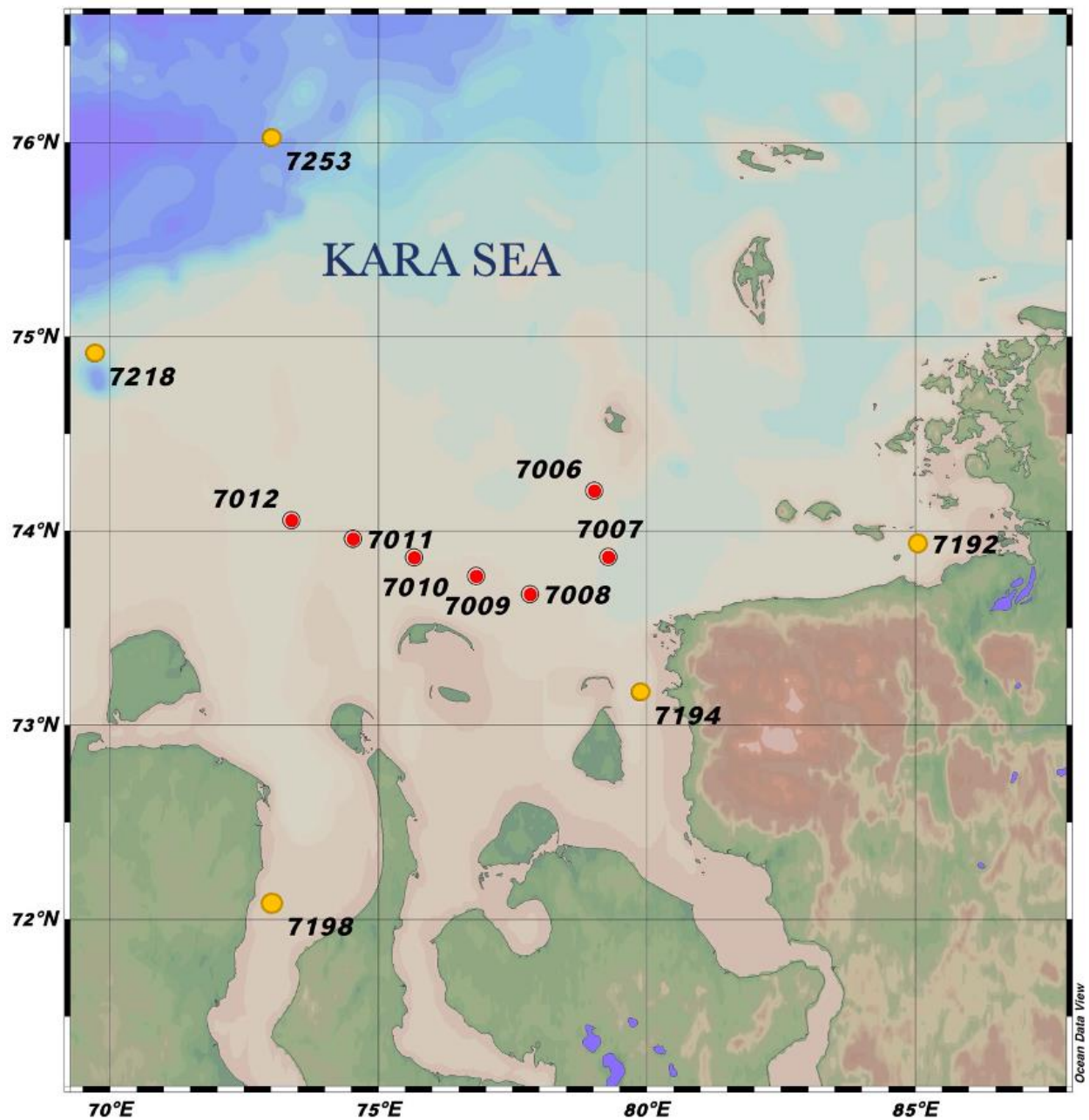
Figure 3.3: A zoom in on Figure 3.2, this map shows both sample locations from 2021 (yellow) and 2020 (red).
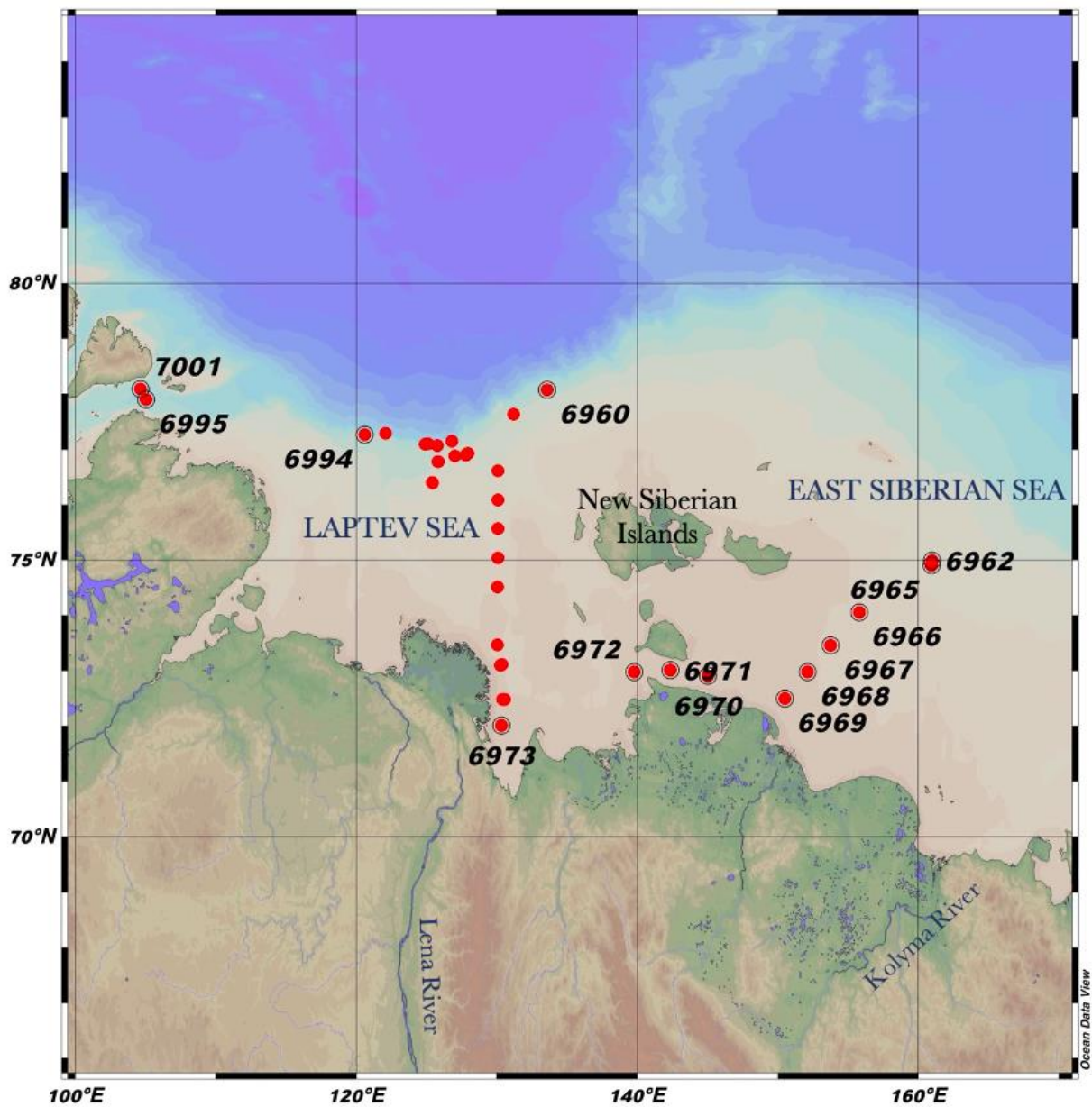
Figure 3.4: A map of sample stations from the Laptev and the East Siberian Sea. Station 6963 and 6964 are not shown on the map as they are between station 6965 and 6962.
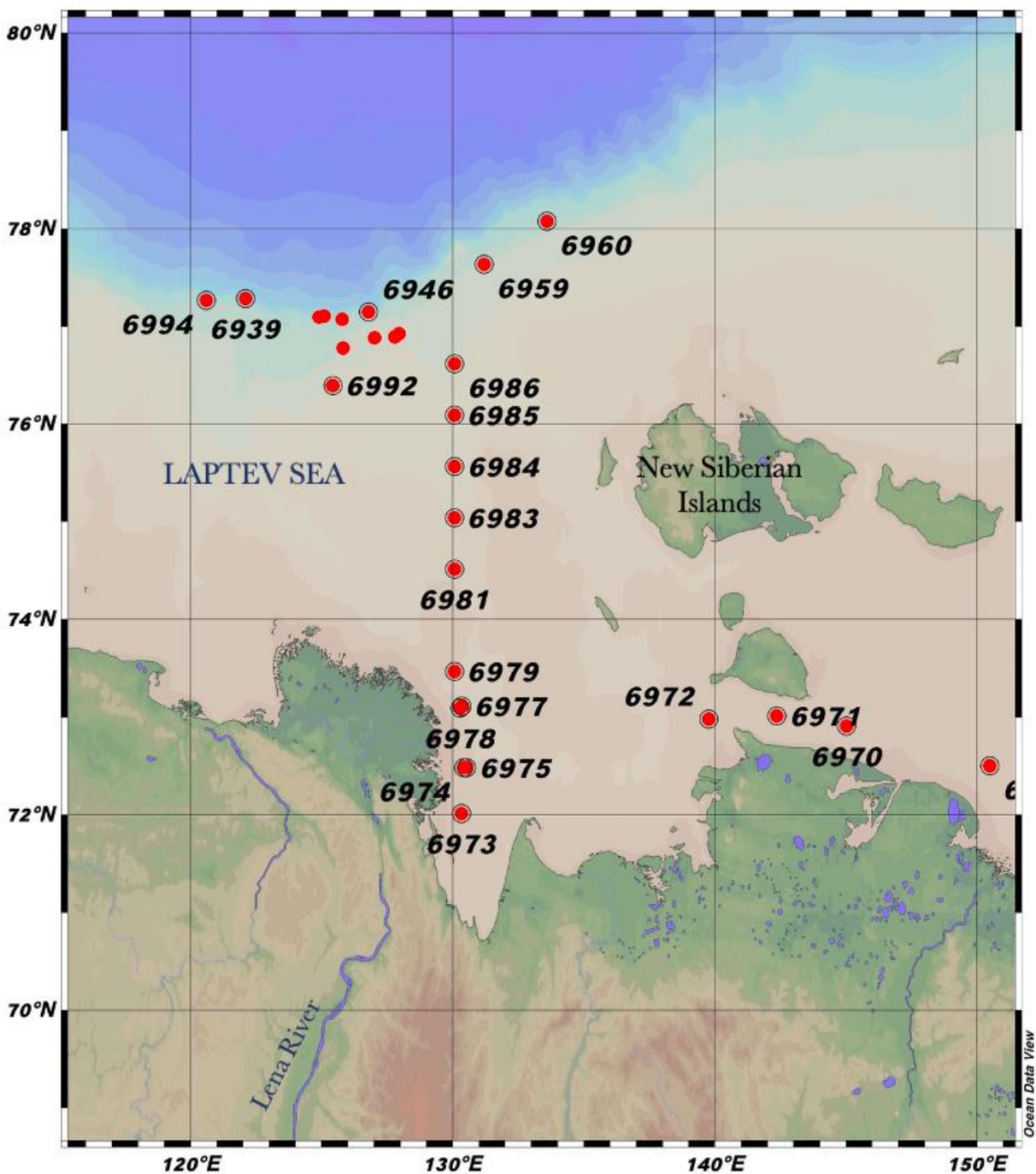
Figure 3.5: A zoom in on Figure 3.4, a further zoom in on the unnamed stations can be seen in Figure A.1 in Appendix A.

A Russian team did the sampling. Hence the following description is based on information sent from the Russian team via email. Sampling in 2020 was taken using a box corer. After the box corer was lifted onto the boat deck, the samples were cut using a plastic tube, and the tubes were brought to the ship's laboratory. In 4-8 hours, the sediments were divided into pieces at intervals

ranging from 1 to 4 cm, which were then packed and sealed in plastic bags. In 2021 the sampling was done using a multi-corer. Figure 3.6 shows a picture of the multi-corer being lowered into the ocean, and Figure 3.7 shows one of the multi-corer's tubes with sediment. The multi-corer consists of 8 tubes where one tube was brought to the ship's laboratory and handled in the same way as the samples from 2020, except for sampling the final block-section samples in plastic tubes with a lid instead of plastic bags.

The depth of each sampling location was noted. The pH and temperature were measured directly after sampling. Sampling was done according to ISO 5667-19, which states that sampling should be done using plastic equipment if the target analyte is a metal (ISO, 2004). The samples were stored in a freezer during transportation and were sent to Trondheim, Norway, from Russia. In Trondheim, the samples were put in the freezer (-22 °C) until analysis.

Figure 3.6: Picture of the multi-corer being lowered into the ocean. The picture is taken from sample station 7192 on the 7th of October 2021.
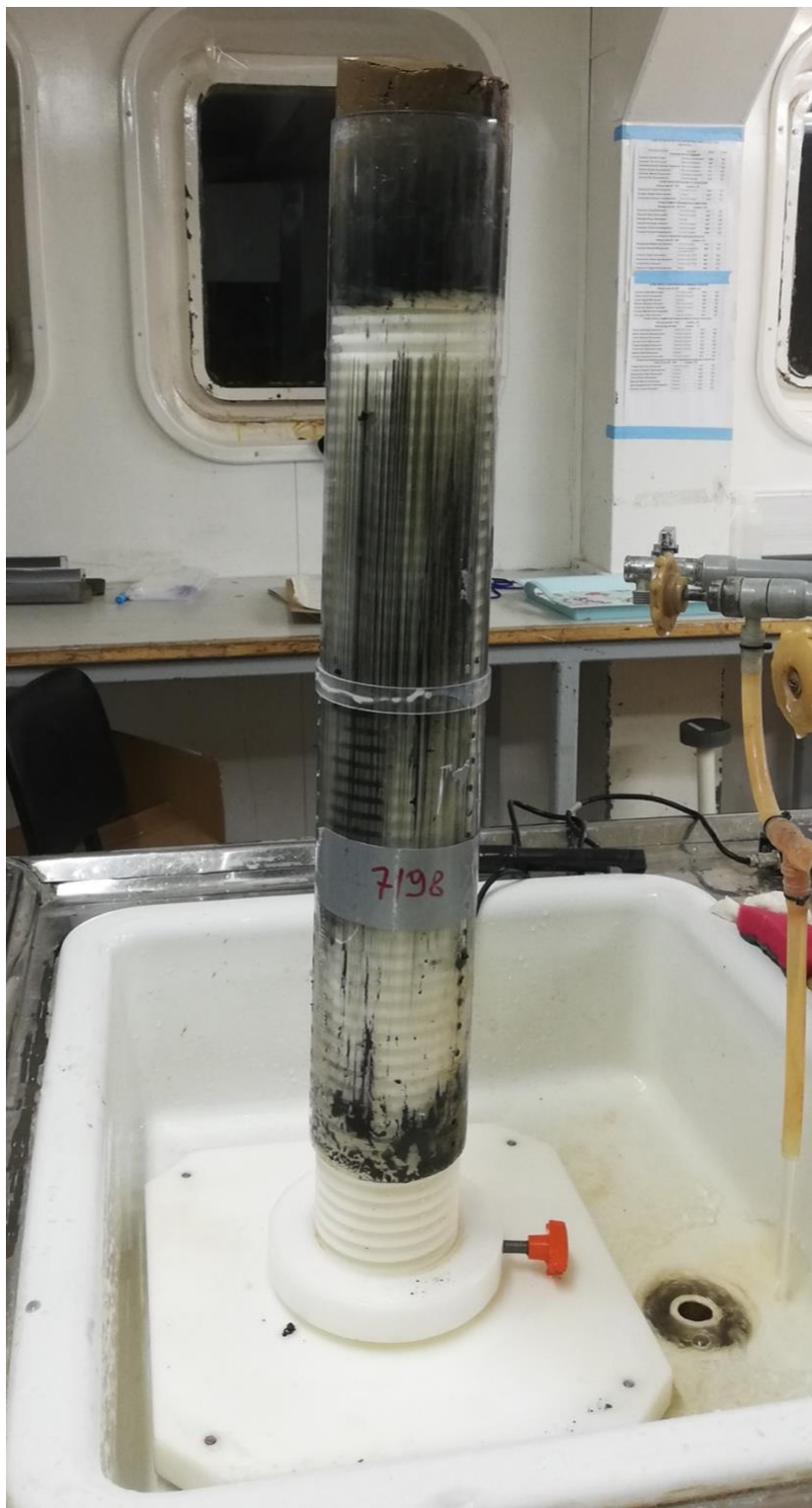
Figure 3.7: Picture of one of the tubes from the multi-corer with sediments. The picture is taken from sample station 7198 on the 10th of October 2021.

3.2 Sample Preparation

All the equipment used for sample preparation was washed with 1,2 M ultra-pure HNO_3 and MilliQ water to prevent contamination. In addition, all sample preparation was done inside a laminar flow chamber under low clean airflow to avoid contamination.

The samples from 2021 were frozen in 50 mL tubes after sampling. The samples were subsampled into smaller tubes (25 mL) to reduce the freeze-drying time. These tubes were cleaned with 1 M HNO_3 for approximately 12 hours and then rinsed three times with MilliQ water. The frozen sediment samples were thawed in a refrigerator to the point where approximately 15 mL of sediment could be transferred with a plastic spatula. For the samples with a cracked lid, the first 1,5 cm of the sample was removed before subsampling. The subsampled tube was then put back into the freezer for at least 24 hours, ensuring the entire sample was frozen before freeze-drying.

The samples from 2020 were sampled in plastic bags. First, these bags were weighed and cut open using a ceramic knife to avoid contamination. Then the samples, still inside the plastic bag, were put in larger plastic cups so that the hole in the plastic bag pointed upwards. Afterwards the samples were frozen in the freezer (-22 °C) for 24 hours before freeze-drying.

The samples were freeze-dried for at least 24 hours until no moisture could be observed. Before the freeze-drying, all the samples were covered with parafilm. The parafilm was poked with holes using a plastic pipette-tip. This was to minimize contamination and still ensure evaporation in the freeze dryer. All the samples were weighed before and after the freeze-drying (Table B.1 and B.2 in Appendix B). After freeze-drying, the samples were homogenized using a mortar and pestle. The mortar and pestle were washed with 1,2 M HNO_3 and MilliQ water three times before each sample-grinding, and the homogenized samples were transferred to new acid-washed 25 mL plastic tubes.

3.3 Analysis of Samples

The total mercury (THg) determination was done using the Direct Mercury Analyser (DMA-80) EVO Milestone instrument. The sediment samples were measured on the measurement-parameter "sediment". The instrument calibration and analytical procedure were conducted according to the EPA 7473 protocol (EPA., 1998).

The EPA 7473 protocol states that solid samples are to be weighed out to ± 0.001g onto a tared sample boat and then be inserted into the instrument, ensuring minimal contamination. Approximately 0,05g of the sediment samples were weighed out into quarts or nickel boats using a plastic spatula that was cleaned with 1,2 M HNO_3 and rinsed three times with MilliQ water.

The sample boat was then transferred into the instrument using a plastic tweezer. The number of samples analysed on each run was between 10 and 20. For every new run/day, a new calibration curve was made with standards containing 0, 0.5, 1, 3, 5, and 10 ng/g Hg. The DMA-80 instrument automatically calculates the concentration using the created calibration curve and the peak-heights from the absorbance cells.

The standards making the calibration curve were prepared from a 1ppm BrooksRand Total Mercury Standard in HNO_3. The preparation of the standards was done in a clean lab. All prepared standards were made with MilliQ water and 2% v/v double-distilled HCl, put in combusted borosilicate amber glass bottles and stored in a fridge (4 °C). The prepared standards contained 0, 1, 3, 5, and 10 ng/g of total Hg. In accordance with the EPA 7473 method, calibration standards were made by measuring out 100 μL of the prepared standards onto a tared sample boat using a 200 μL pipette. This was then weighed and transferred to the instrument. The only exception was for the 0,5 ng/g calibration standard, where 50 μL was measured out from the 1 ng/g standard.

The true blanks consisted of MilliQ water and 2% v/v HCl, boat blanks refer to empty sample-boats, and blind values refer to the machine running without a sample-boat. Before each run, a set of blind values, boat blanks, and true blanks were analysed, and a new calibration curve was conducted using standards ranging from 0 ng to 10ng in accordance with the EPA 7473 protocol. The liquid standards were analysed in quartz boats, and these quartz boats were run as boat blanks before the standards to ensure that they were clean. After analysing the samples, a new set of blind values were analysed to ensure that the signal was not affected by residue from the previous samples. As the EPA 7473 protocol states, each sample run should include a reference standard, and this standard should be within 20% of the true value, or else the samples should be reanalysed (EPA., 1998). Therefore, each sample run was ended by analysing the certified reference material BCR-277R twice. After each run, all the sample boats were cleaned with MilliQ water three times. Table 3.1 and Table 3.2 show the standard deviation, mean, highest and lowest value from the CRM and blanks, respectively.

Table 3.1: Shows the calculated values of Hg from 26. runs of the CRM BCR-277R.

Count	26
Average (ng/g)	137,86
Median (ng/g)	135,79
Minimum value (ng/g)	128,18
Maximum value (ng/g)	156,03
Standard deviation (Given) (ng/g)	17
Standard deviation (Calculated) (ng/g)	6,72
QC value (Given) (ng/g)	128

Table 3.2: The calculated values of Hg from all the blank boats

Count	45
Average (ng)	0,0162
Minimum value (ng)	0,0117
Maximum value (ng)	0,0366
Standard deviation (ng)	0,0042
Limit of detection (ng)	0,0126
Limit of quantification (ng)	0,0421

Two samples were collected randomly from the last two runs and duplicated. The re-analysations of these samples are so-called "pseudo replications," as the same sample is analysed several times, but will be referred to as duplicates from here on out. The standard deviation from the duplicates was calculated. The last run included one sample from the first three runs to see if the DMA-80 had a shift, and the standard deviation was calculated. In addition, the standard deviation was taken from all the boat blanks and the certified reference material of all individual runs. Finally, the mean of all the blanks was subtracted from sample Hg concentrations to correct for possible mercury contamination during the analysis.

To get a good overview of the samples' concentration and compare them with their location, "Ocean Data View" (ODV) was used. ODV is a software package for exploring and visualizing oceanographic and geo-referenced data. It can display original data points or gridded fields based on the original data. However, it should be noted that the gridded fields are data products, and small scale or extreme features in the data may be modified or lost as a consequence of the gridding procedure (Alfred Wegener Institute, 2022).

4 Results

In total, 97 different samples were analysed on the DMA-80 instrument taken from 60 different sampling locations. Tables C.1 – C.12 in Appendix C shows the concentration of Hg in ng/g. Table 4.2 shows the average, median, highest, lowest, and standard deviation from all the samples, and 2020 and 2021 isolated. All the boat blanks (Table C.13) were used to calculate LOD and LLOQ, and were found to be 0,0126 ng and 0,0421 ng, respectively (Table 3.2). For the samples taken from station 6968 and 6970 the average concentration from the three runs on the DMA-80 is used. For the sample taken from station 7253 from the core depth 23 – 30 cm the average from the two runs on the DMA-80 is used, and for the sample from station 7192 from the core depth 1 – 2 cm the average from three runs on the DMA is used. The Hg concentration of the duplicates can be seen in Table 4.2.

The certified reference material (CRM) BCR-277R has a certified value of 128 ng/g Hg with a given standard deviation of 17 ng/g (Table 3.1). The CRM was analysed 17 times on the DMA, and 9 previous runs from January 2022 were included. From the 26 analyses of the CRM (Table C.14), the average was 137,86 ng/g, three of the measured standards were above 128 + 17 ng/g Hg and none were below 128 ng/g.

Table 4.1: The calculated values of Hg from all samples, 2020 and 2021 isolated, from all the surface samples, and surface samples from 2021 isolated. Duplicates are included in this table.

	All samples	2021	2020	All Surface Sediments	2021 Surface Sediments
Count	105	52	53	66	13
Average (ng/g)	37,353	38,861	35,875	36,461	38,878
Median (ng/g)	35,190	34,855	36,905	36,358	33,583
Minimum value (ng/g)	1,975	11,598	1,975	1,975	9,407
Maximum value (ng/g)	76,778	76,778	68,425	70,498	70,498
Standard deviation (ng/g)	17,091	15,864	18,244	18,130	18,171

Table 4.2: The duplicates and the date of analysis, Hg concentration, calculated average, standard deviation, and relative standard deviation. The average of the five STDs and RSTDs are calculated to be 0,649 ng/g Hg and 1,34 %, respectively.

Duplicates	Date analysed	Hg (ng/g)	Average (ng/g)	Standard deviation (ng/g)	Relative STD (%)
7253	09.02.2022	24,300			
(23 – 30 cm)	29.03.2022	23,825	24,063	0,336	1,40
7247	10.02.2022	27,381			
	29.03.2022	29,423			
	29.03.2022	30,231	29,012	1,469	5,06
7192	14.02.2022	36,469			
(1 – 2 cm)	29.03.2022	35,206			
	29.03.2022	35,091	35,589	0,765	2,15
6968	29.03.2022	20,915			
	29.03.2022	20,672			
	29.03.2022	21,039	20,875	0,187	0,90
6970	22.03.2022	36,958			
	22.03.2022	36,922			
	22.03.2022	36,092	36,657	0,490	1,34

4.1 Sediment Cores

The samples taken in 2021 include 47 samples, where 46 are sediment core samples from 10 different locations. Figure 4.1 shows the distribution of Hg concentrations plotted against the depth of the core-samples, and Figure 4.2 shows the linear regression for all the samples plotted against the depth. Figures 4.3 and 4.4 show a graphic representation of each core sample, including the exact depth interval from the cores. Note that the depth interval varies for each core. The highest Hg concentration is 76,79 ng/g, which is measured from station 7249 at 3 – 10 cm depth, and the lowest concentration is 11,60 ng/g, which is measured from station 7198 at 0 – 0,5 cm depth.

The sediment core samples vary in depth intervals and the number of samples taken from each sampling station. The highest variation in concentration along the depth is 32,56 ng/g from station 7249, followed by station 7250 with 24,03 ng/g, and the lowest variation is 1,53 ng/g from station 7212, followed by station 7218 with 4,65 ng/g. The general trend using linear regression on each individual core sample is that the concentration of Hg decreases with depth, except for the core samples taken from stations 7198, 7212, and 7218. Figure 4.2 shows the linear regression for all core samples and there is an increasing trend with decreasing depth of the cores. The equation for the linear regression in Figure 4.2 is $y = -0,0599x + 11,376$, and $R^2 = 0,0113$. The deepest core goes 37 cm down into the sediments (station 7222), and the shallowest goes only 7 cm (station 7198) as can be seen from Figures 4.3 and 4.4.
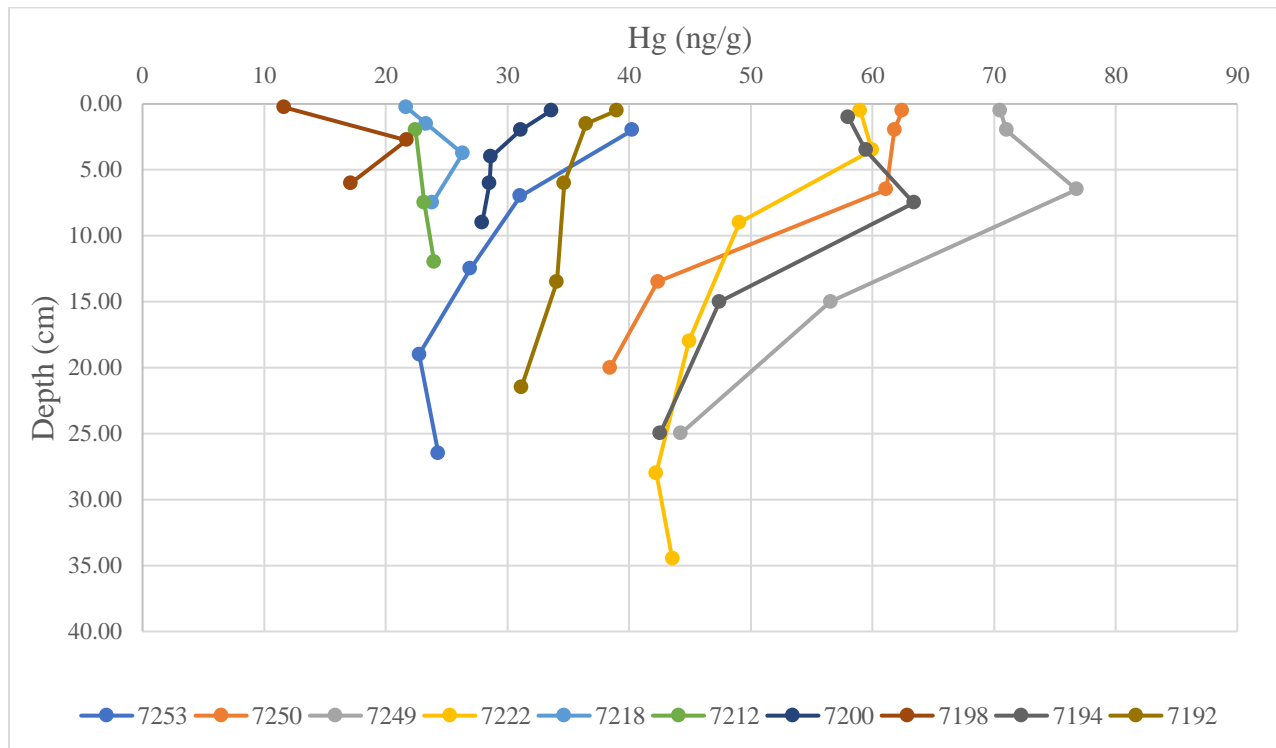
Figure 4.1: Representation of the depth profile taken from all stations from 2021 except for 7247. The y-axis shows the depth of the sediment core sample, and the x-axis show the concentration. The depth is plotted as the middle value of the core sample. The different colours represent the different sampling locations, and each station is given at the bottom of the graph.
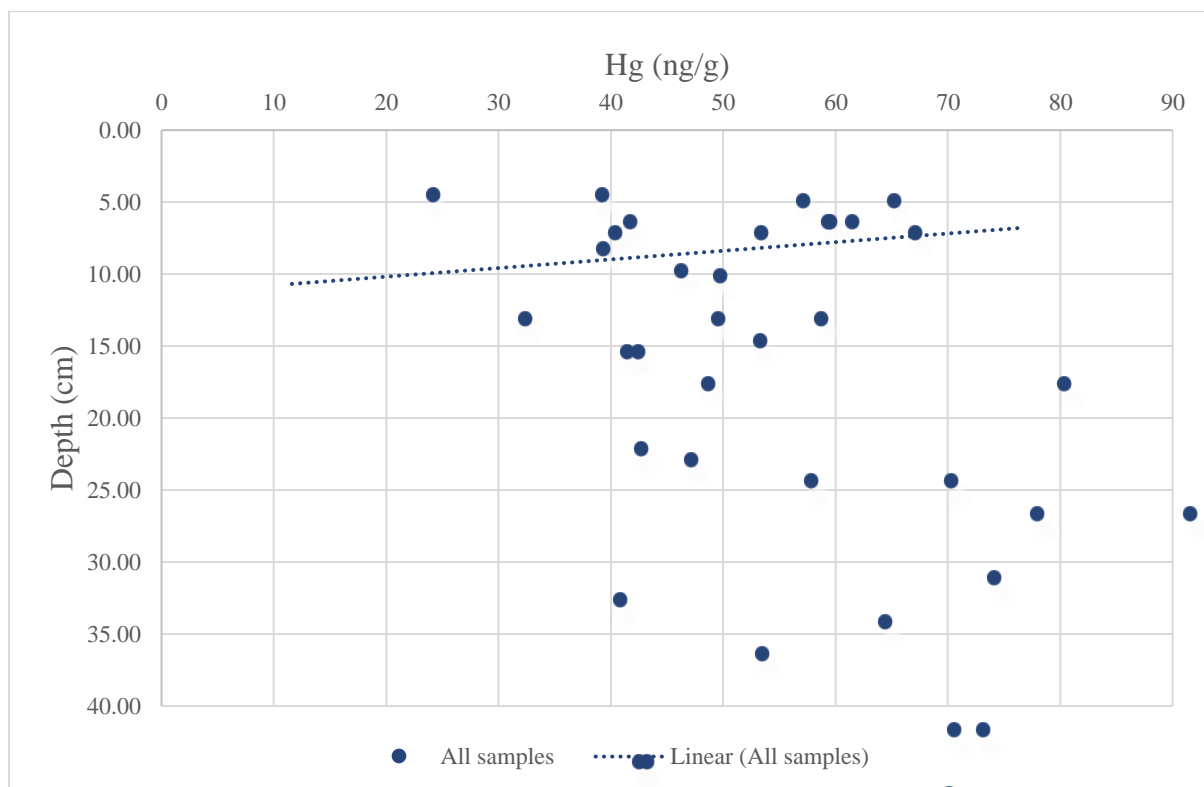
Figure 4.2: Representation of the depth profile taken from all stations from 2021 except for 7247. The y-axis shows the depth of the sediment core sample, and the x-axis show the concentration. The depth is plotted as the middle value of the core sample. The equation for the linear regression is y = - 0,0599x + 11,376, and R^2 = 0,0113
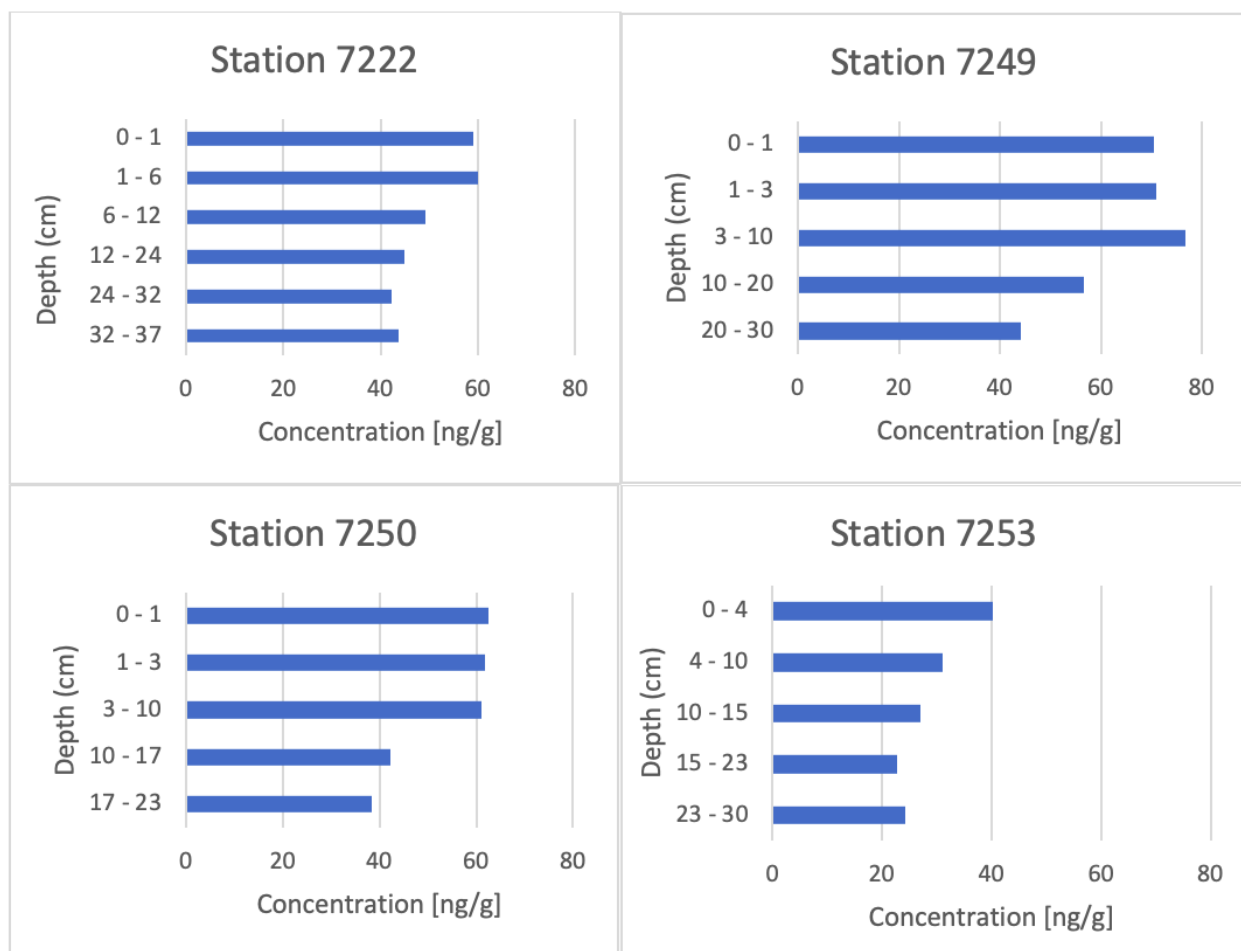
Figure 4.3: Representation of the sediment core samples where the water column depth exceeds 100 m. The y-axis represents the different depth intervals, with the surface sediment layer at the top. Note that the depth intervals vary. The x-axis represents the concentration of Hg in ng/g. The depth of the water column for each station can be seen in Table 5.2 in the appendix.
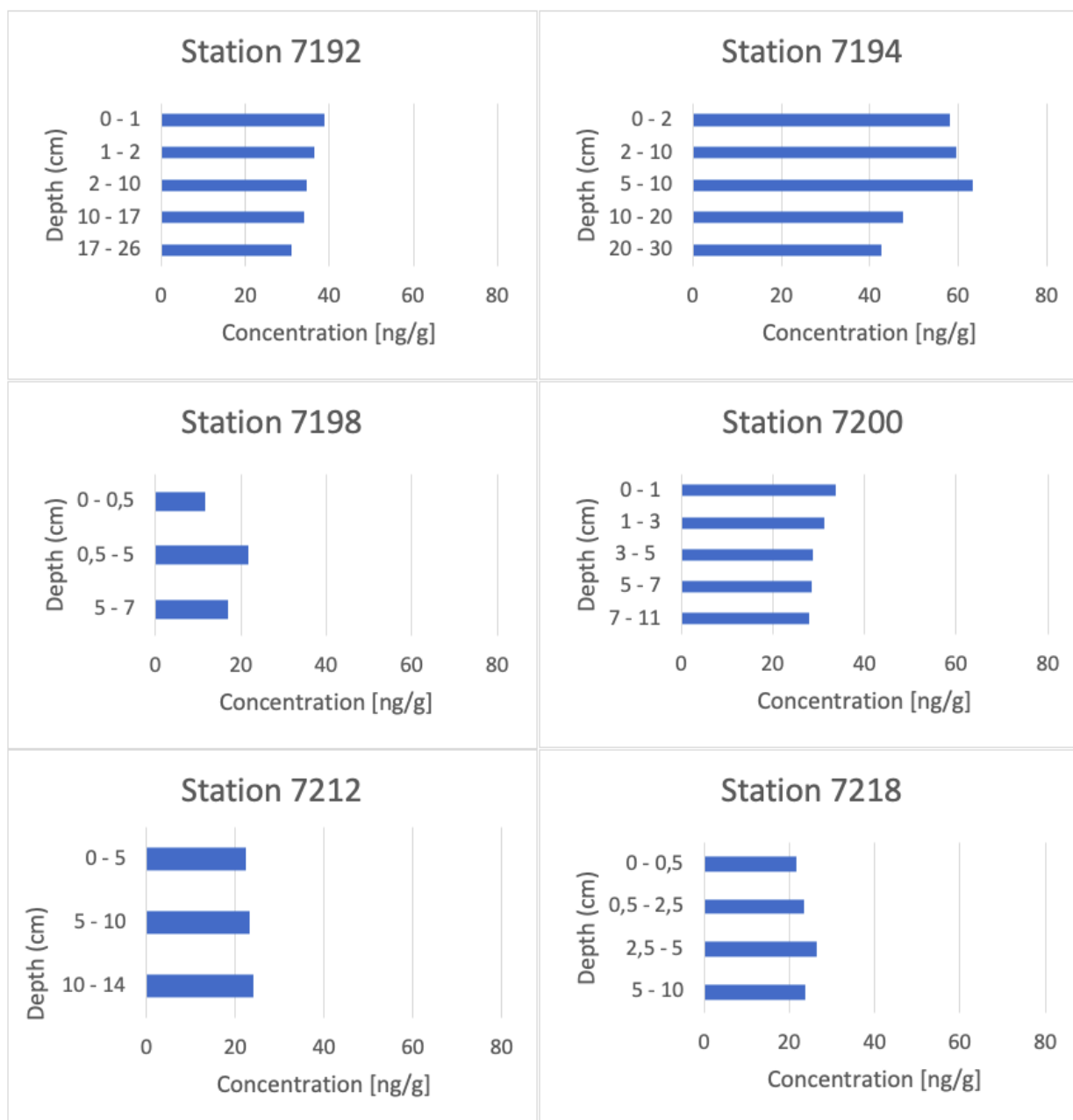
Figure 4.4: Representation of the sediment core samples where the water column depth is below 100 m. The y-axis represents the different depth intervals, with the surface sediment layer at the top. Note that the depth intervals vary. The x-axis represents the concentration of Hg in ng/g. The depth of the water column for each station can be seen in Table 5.2 in the appendix.

4.2 Surface Sediments

The sampling from both 2020 and 2021 includes sediment surface samples from 60 different locations/stations. Concentrations of THg from the surface sediments ranged from 1,99 ng/g at station 7011 to 70,52 ng/g at station 7249. Figure 4.5 shows the sampling locations with colour-coded dots representing Hg concentration, while Figure 4.6 shows a gridded field based on the original data. Figures 4.7 – 4.9 shows each sea individually with colour coded dots representing the THg concentration. Figures 4.10 – 4.12 shows the depth of the water column plotted against the concentration of Hg. The sample from station 7247 is not included in Figures 4.10 and 4.11, as information regarding the depth of the water column was not given. Figure 4.10 show that the sampling location with the highest Hg concentration is also the deepest.
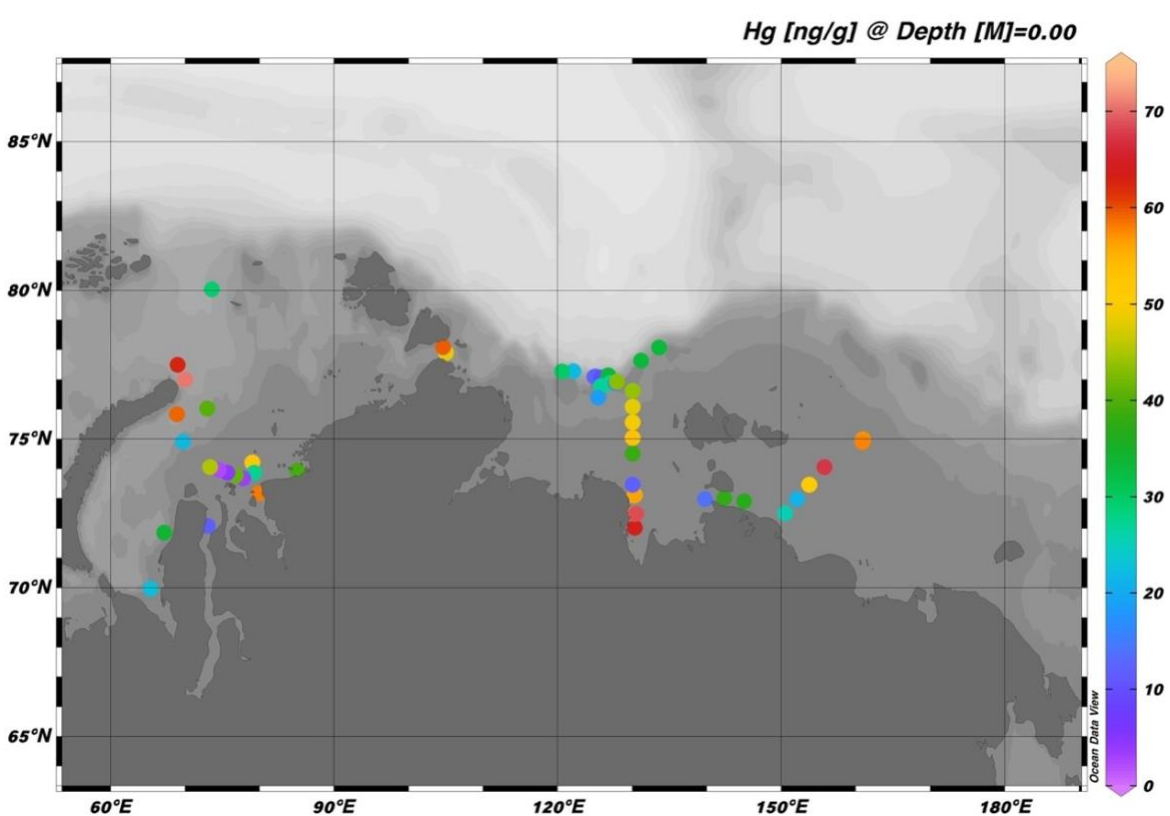
Figure 4.5: Map of all the sample locations and the surface sediment concentration of Hg in ng/g as can be seen on the colour of the dot.
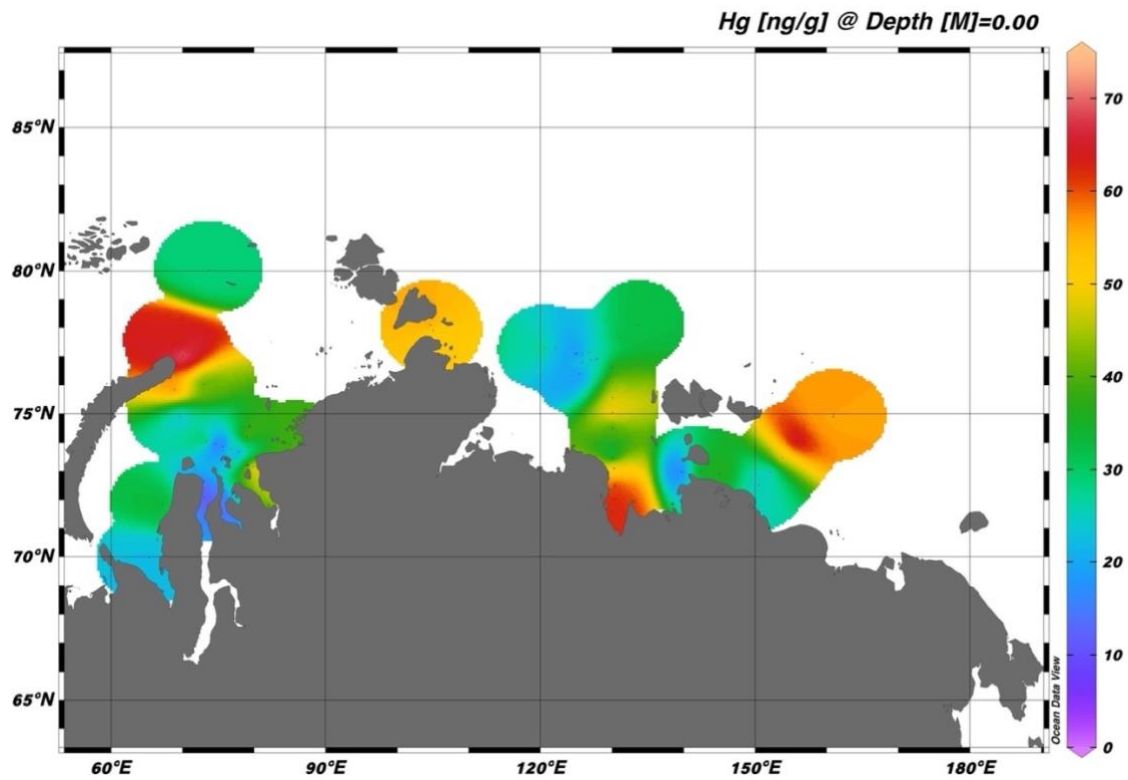
Figure 4.6: Map of the surface sediment concentration of Hg in ng/g shown as gridded fields.
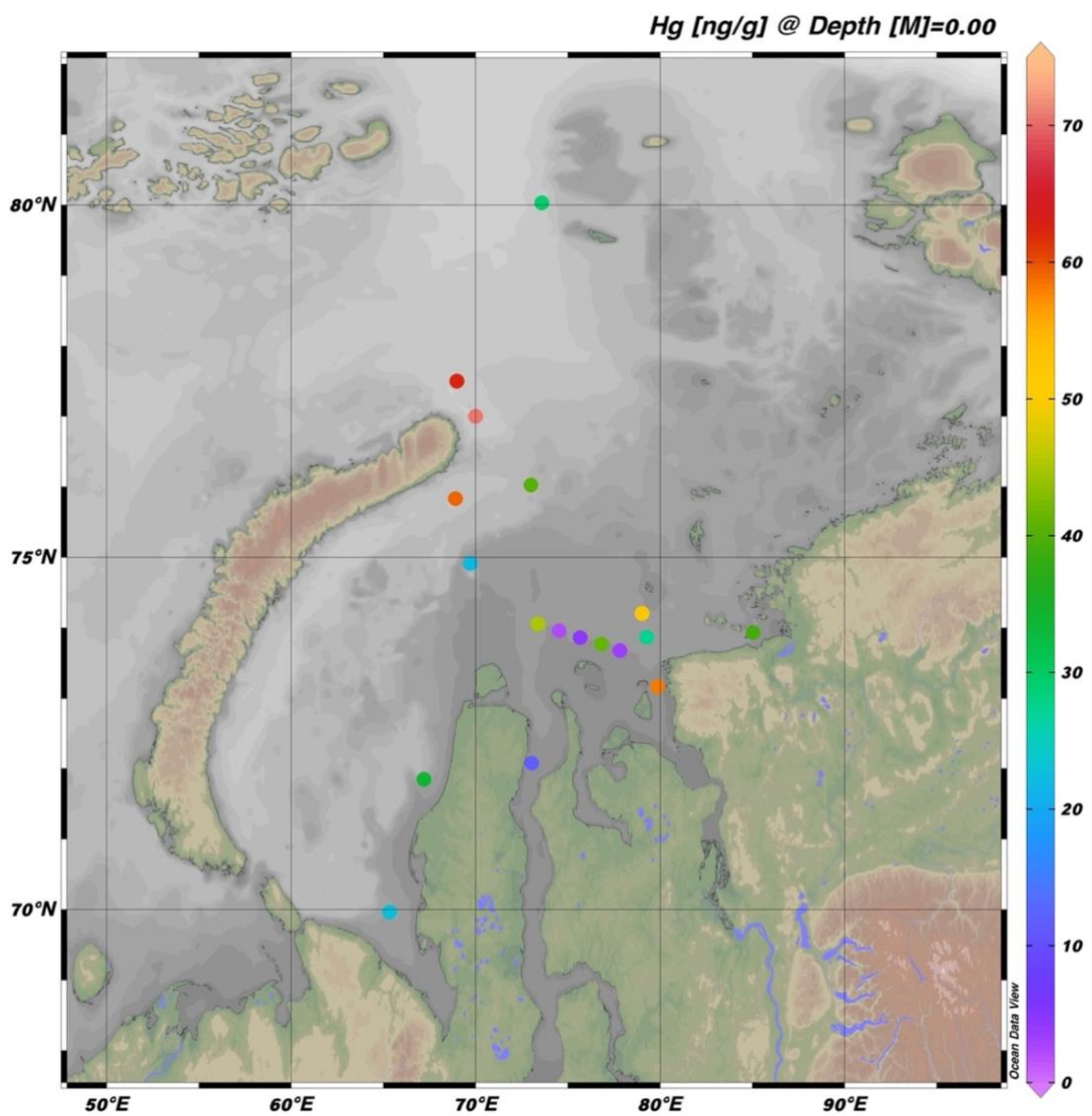
Figure 4.7: Map of all the sample locations in the Kara Sea and the surface sediment concentration of Hg in ng/g as can be seen on the colour of the dot.
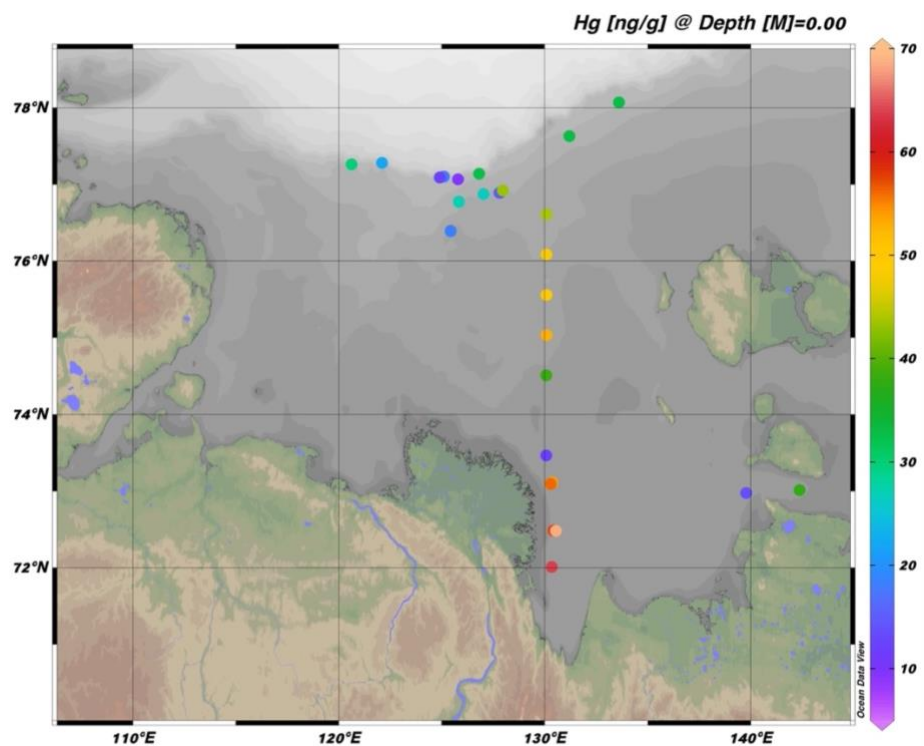
Figure 4.8: Map of all the sample locations in the Laptev Sea and the surface sediment concentration of Hg in ng/g as can be seen on the colour of the dot.
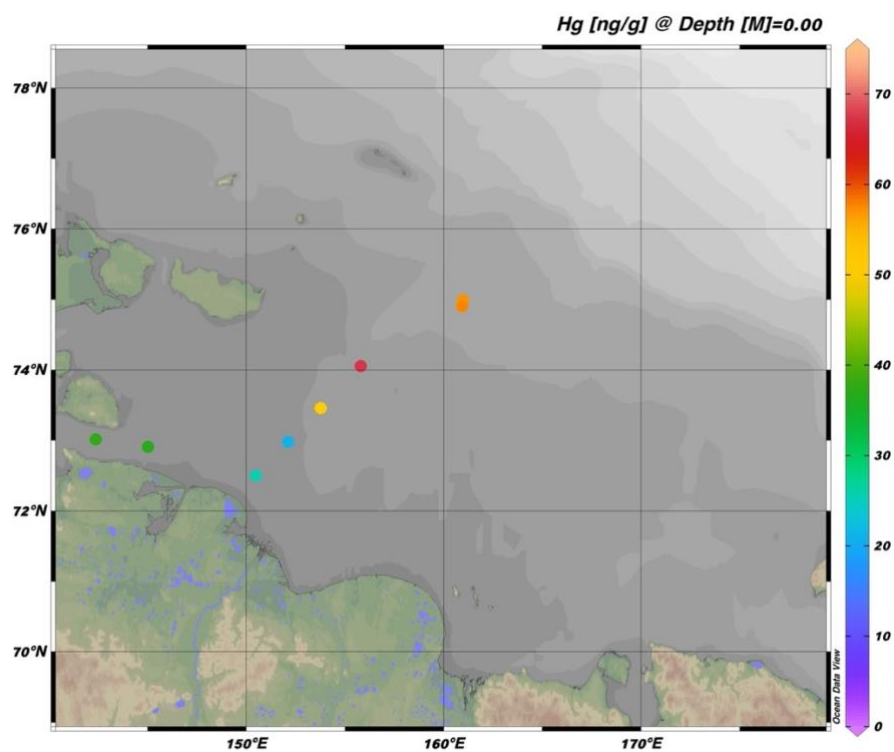
Figure 4.9: Map of all the sample locations in the East Siberian Sea and the surface sediment concentration of Hg in ng/g as can be seen on the colour of the dot.
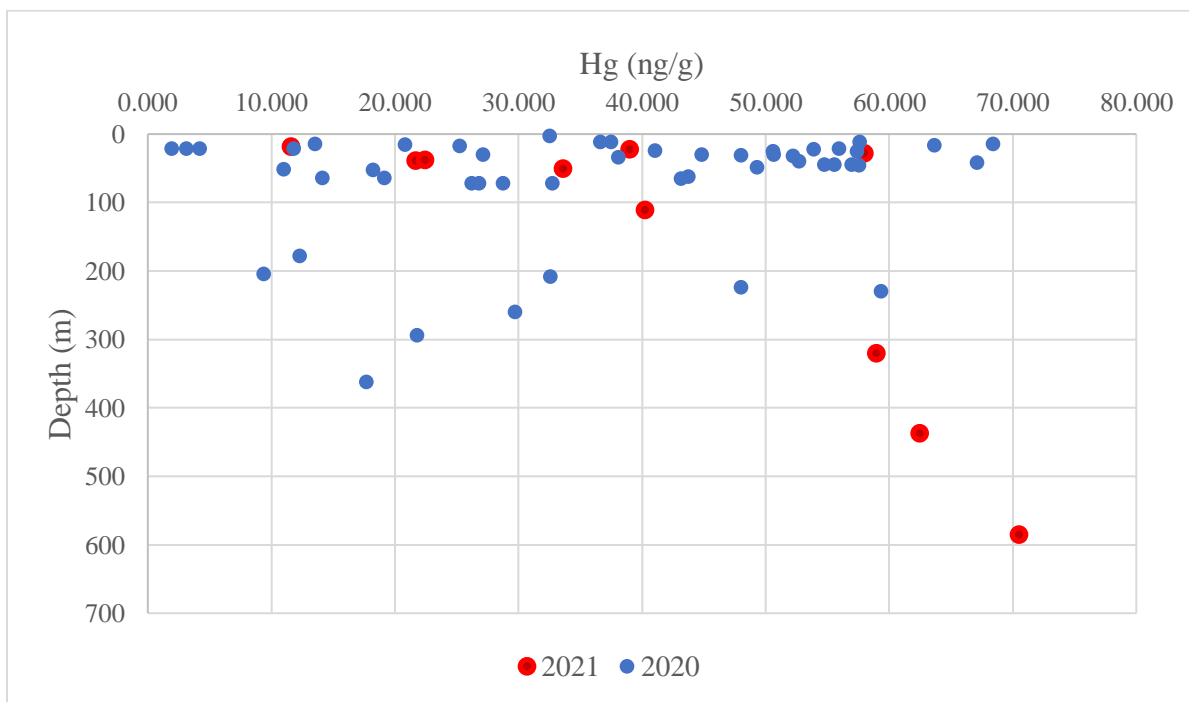
Figure 4.10: Graphic representation of surface sediment samples from 2020 (blue) and 2021 (red), where the concentration of Hg on the x-axis is plotted against the depth of the water column on the y-axis.
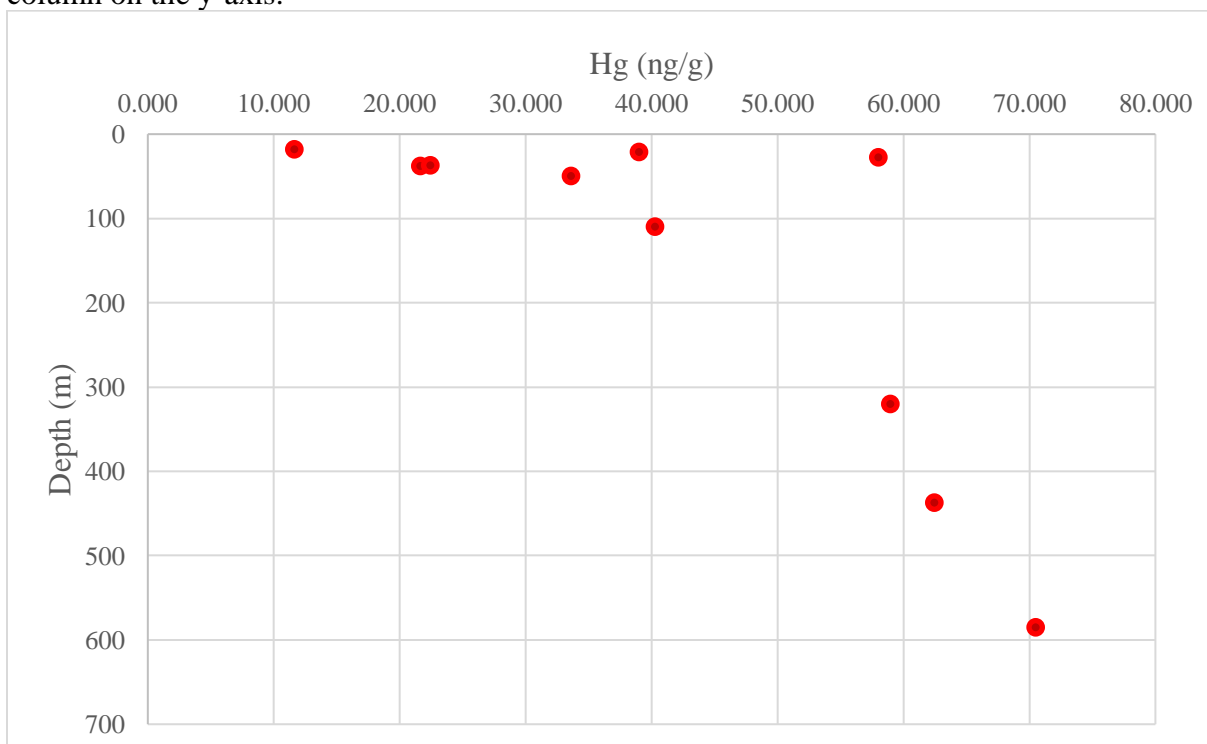
Figure 4.11: Graphic representation of surface sediment samples from 2021 where the concentration of Hg on the x-axis is plotted against the depth of the water column on the y-axis.
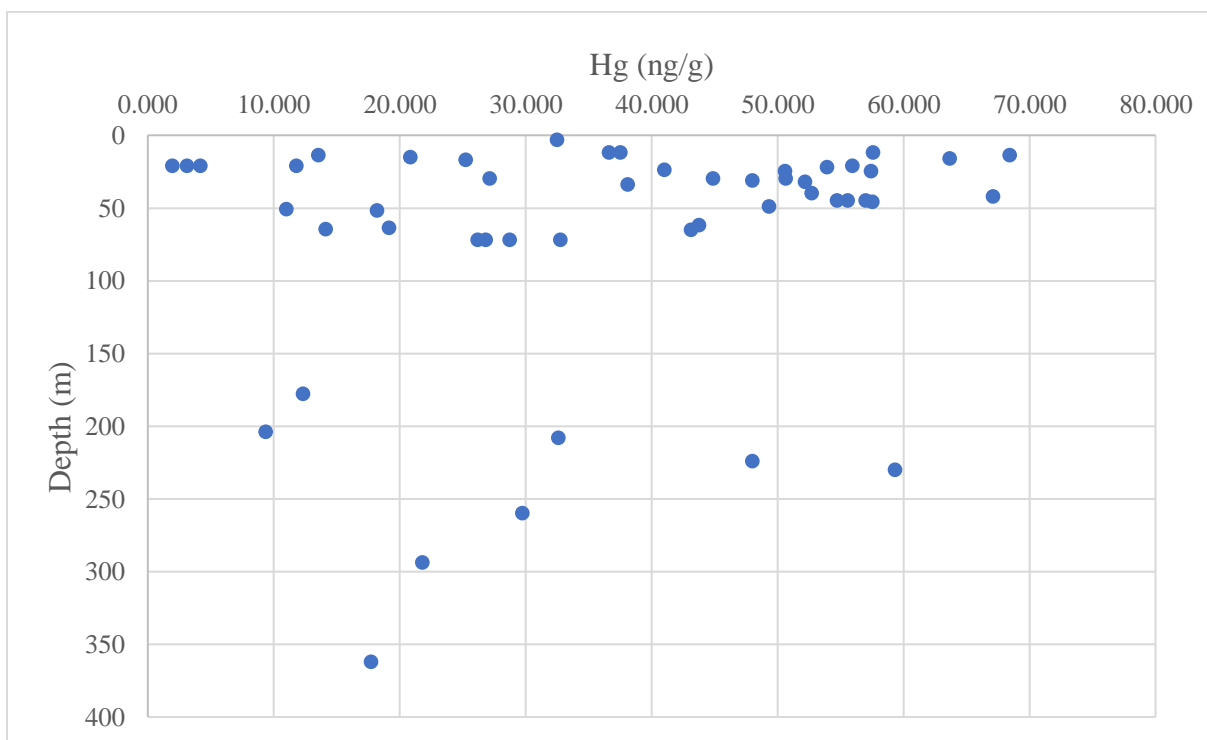
Figure 4.12: Graphic representation of surface sediment samples from 2020 where the concentration of Hg on the x-axis is plotted against the depth of the water column on the y-axis.

5. Discussion

5.1 Quality Assurance and Quality Control

5.1.1 Sampling

As Batley (1999) stated, it is ideal to have as much control as possible of each step in analysing environmental samples. The samples in this thesis are sampled by a separate team in Russia and are prepared and analysed by the author of this thesis. This has had some implications, and some information regarding the samples has been difficult to acquire. For example, the visible anoxic and oxic segments of the sediment cores. In addition, the coupling of sediment samples with the information regarding the samples has not always been apparent, and it seems likely that not all the samples taken during the two cruises have found their way to Trondheim. Meaning that the samples included in this thesis represent a smaller picture than that that was originally planned for by the sampling team. The number of samples analysed is below 100 and is spread over a large area. It could be argued that more samples from a narrower area would give a more precise image of the conditions in the sediment.

The two sampling periods do not include the same sampling locations. It could have been interesting to see if the Hg concentrations on the sediment surface would have changed from 2020 to 2021. This could have given information regarding the current rate of mercury deposition onto the sediments. If this were to be done, then the sampling should be done using the same sampling method, as the sampling from 2020 was done using a box-corer while the sampling from 2021 used a multi-corer. The sampling in both 2021 and 2020 was done in October, and it could have been interesting to see if there is a seasonal difference. However, as the seas are frozen for most of the year (Gunnarsson, 2021), the samples could not be collected from different seasons.

5.1.2 Sample Preparation

The samples from 2021 were subsampled before they were freeze-dried. When subsampling, the frozen samples had to thaw to be able to remove the sediment from the original tube. The samples were thawed to a minimum in a fridge. This might have influenced the results as bacteria or other organisms could be active and change the decomposition and speciation of the mercury present. As the samples were measured for the total amount of mercury, this should not affect the result significantly. However, bacteria can reduce divalent mercury to elemental mercury (Coulibaly *et al.*, 2016), and as elemental mercury is volatile it may escape the sample matrix, which could have influenced the results. In 1991 it was estimated that the average evaporation rate of elemental mercury in surface soils is approximately 0,30 ng m^{-2} h^{-1} at 10 °C (Schlüter, 2000). The temperature in the fridge where the samples were thawed was 4 °C, and

they were subsampled at room temperature. The samples were without caps for around 5 minutes, and using Schluter's (2000) estimation, this would result in about 0,025 ng m^{-2} of Hg^{0} to evaporate. As the surface of the tube is substantially smaller than a square meter, the total amount of evaporating Hg^{0} can be considered insignificant. However, a change in speciation during thawing should be considered if these samples are to be analysed for MeHg in the future. Another aspect of the subsampling is that only part of the total sample material was included in the subsampled tube. Therefore, it could be that the subsamples do not give a complete picture of the concentration in the given depth interval.

As the EPA protocol states (1998); a set of blanks, duplicates, and spiked control samples should be included to ensure reproducibility. During the sample preparation, neither a procedure blank nor a method blank was included, and there is no knowledge of field blanks. Therefore, contamination that might arise from the sample preparation, as well as the sampling, is not accounted for.

5.1.3 Data Analysis

The average Hg concentration for the CRM was calculated to be 137,86 ng/g. This is within the given range of 128 ± 17 ng/g Hg, even though it is above the verified value of 128 ng/g. The calculated standard deviation for the BCR-277R values is lower than the given standard deviation, but three samples exceeded the given value of 128 ± 17 ng/g Hg. The calibration points that were made in each run ranged from $0 - 10$ ng, and one could expect the CRM-signal to exceed this causing the calibration to be poor above this point. However, only two of the 26 CRM values exceeded the signal of 10 ng on the DMA-80 (Table C.14 in Appendix C). The analytical methods used for certification of the BCR-277R do not include DMA-80 (IRMM, 2007).

Table 3.2 shows the average ng of Hg for all the blanks. Compared with the minimal working range of the DMA instrument, which is 0,05 ng, the average of the blanks and the calculated LOD and LOQ are accepted values. All the sediment samples were above the LOD and LOQ. The blanks include both blanks of nickel and quartz boats. When the boat blanks were analysed the nickel boats did not deviate from the quartz boats, and as the sediment samples were measured in both quartz and nickel, this was not differentiated.

A spiked control sample was not included to adjust for possible matrix effects. However, the operating principle of the DMA-80 eliminates most matrix effects (Gueu, Ouffoué and Digbéhi, 2021). Duplicates were only included in the last two runs. The samples that were duplicated are shown in Table 4.2. The standard deviation (STD) of the duplicates ranges from $0,187 - 1,469$ ng/g, and the relative standard deviation (RSTD) ranges from $0,90 - 5,06$ %. The highest STD and RSTD is calculated from the duplicates of sediment samples from station 7247, and these

were analysed on different days. As shown in Table 4.2, the first measurement from sample 7247 gave a significantly lower value than the last two duplicates measured on the same day. However, the highest STD and RSTD is more than twice the amount of the average standard deviation from all five duplicates (0,649 ng/g Hg and 1,34 %).

5.2 Core Samples

All the surface sediment values from the core-samples show higher Hg concentrations than the deepest sample, except for the core samples taken from stations 7198, 7212, and 7218 (Figures 4.1, 4.3 and 4.4). Figure 4.2 show a trend using linear regression of decreasing THg concentrations with increasing depth with the low R^2 value of 0,0113, indicating that the data points fall far from the regression line. The core samples from stations 7198, 7212 and 7218 shows a deviation from the general regression line in Figure 4.2. However, the core samples from station 7198 and 7218 are the shallowest, and all three locations have only three depth interval measurements. From the information that was sent from Russia regarding the samples, there seemed to have been several core depths that have been lost during transportation to Norway. Meaning that Figures 4.1 – 4.4 might not provide an accurate image of the distribution of Hg in sediment cores. It would be interesting to see if the trend would differ with deeper sediment cores available from stations 7198, 7212, and 7218.

The sediment cores taken from stations 7250 and 7249 are relatively close to each other and from the northeastern part of the island Novaya Zemlya (Figure 3.1). These two core samples, together with station 7222, have the highest Hg concentration values. Station 7222 is also relatively close to Novaya Zemlya. The northern part of Novaya Zemlya is largely covered with ice and mountain glaciers, which are experiencing surface melting due to seasonal change, which has itself increased in later years due to climate change (Melkonian *et al.*, 2016). Therefore, the runoff from the glaciers could cause increasing Hg concentrations at this site.

5.2.1 Sedimentation Rate

To provide information on the change in total mercury concentration over the years, the sedimentation rate must be calculated. As the sedimentation rate varies with depth and location, the rate must be calculated from each sample station to give an accurate depiction. Due to the limited amount of time, the content of ^{210}Pb was not measured for the core samples from the Kara Sea, and consequently, the sedimentation rate using this method cannot be calculated for each core. Therefore, sedimentation rates calculated by earlier studies will be used to evaluate the sediment cores in this thesis. This assumes that the sedimentation rate is even across larger areas, which provides uncertainties. For example, a study on mercury in sediments in the East Siberian Sea calculated the sedimentation rate from one single core, with the depth of the water column being 247 meters, to be 0.45 mm/year (Aksentov *et al.*, 2021). The core from this study

lies in the open ocean of the East Siberian Sea, and the nearest sampling station for this thesis would be stations 6963 – 6965, where the water column depth is 45 meters. The samples taken from stations 6963 – 6965 were not sampled as core samples. Different regions of the Arctic Ocean may vary considerably in sedimentary environments regarding parameters such as provenance, background sedimentation rates, and local sediment redistribution (Polyak and Jakobsson, 2011). This means that this sedimentation rate would not be accurate to use on the collected cores as they are taken from a different location where sediment conditions could vary significantly. However, the vertical distribution of the core sample from Aksentov *et al.* (2021) analysis can be evaluated with the THg concentrations of these cores. Aksentov *et al.* (2021) found that the concentration of mercury increased from 24 ng/g at 27 cm depth to 55 ng/g at the sediment surface layer. It was also found that at depths below 11 cm, the Hg content had an average of 28 ng/g, and it gradually increases from this depth. Based on the sedimentation rate of 0,45 mm/year, the sediment interval between 0 and 5,5 cm depth was accumulated in the last 100 years, and the deeper sediments are thought to be the natural background Hg concentration (Aksentov *et al.*, 2021). For the core samples in this thesis, the average Hg concentration from depths below and above 10 cm is shown in Table 5.1. This thesis's core samples have fewer depth intervals than the compared core samples from the East Siberian Sea. Still, all cores that have measurements below 10 cm show higher average values in the top sediment layer than for the sediment layers below 10 cm, except for station 7212. The sedimentation rate of these cores must be calculated to evaluate if the average concentration of Hg below 11 cm can be considered natural background content.

Table 5.1: Shows each core station and the average Hg concentration in ng/g from above and below 11 cm. The depth of each core can be seen in table 5.2. Core samples from station 7218, 7200, and 7198 do not include sediment layers below 10 cm.

Station	Average Hg above 10 cm depth (ng/g)	Average Hg below 10 cm depth (ng/g)
7253	35,64	24,57
7250	61,78	40,37
7249	72,76	50,39
7222	55,99	43,57
7218	23,77	-
7212	22,78	23,96
7200	29,93	-
7198	16,80	-
7194	60,28	44,98
7192	36,40	32,58

A different study done by Rusakov *et al.* (2019) focused on the Kara Sea sedimentation rate, which studied multiple cores finding different sedimentation rates for each location. The

sedimentation rates found in this study are relatively high compared to other estimations (Aksentov *et al.*, 2021; Rusakov, Borisov and Solovieva, 2019; Tesán Onrubia *et al.*, 2020). Two of these findings are of interest as two of the studied locations are relatively near stations from the presented core samples in this thesis. They found that sediment samples located between sampling stations 7249 and 7222 had a sedimentation rate of 1,7 mm/year, and near station 7198, the sedimentation rate was found to be 8,9 mm/year, which also was the highest rate of sedimentation that was found in this study (Rusakov, Borisov and Solovieva, 2019). The sedimentation rates calculated by Rusakov *et al.* (2019) are used for the core samples from station 7253, 7250, 7249, 7222, and 7198, and the calculated depositing years are presented in Table 5.2. Cores from station 7250 and 7253 are included in the table as the location is relatively near compared with the other sample stations.

Table 5.2: Mercury deposits over time using the sedimentation rates calculated from relatively nearby sampling stations sampled and calculated by Rusakov *et al.* (2019).

Station	Water Column Depth (m)	Core Depth (cm)	Sedimentation Rate (mm/year)	Depositing Years	Hg (ng/g)
7253	110	0 – 4	1,7	2021 – 1997	40,24
7253	110	4 – 10	1,7	1997 – 1962	31,04
7253	110	10 – 15	1,7	1962 – 1933	26,92
7253	110	15 – 23	1,7	1933 – 1886	22,72
7253	110	23 – 30	1,7	1886 – 1845	24,28
7250	437	0 – 1	1,7	2021 – 2015	62,44
7250	437	1 – 3	1,7	2015 – 2003	61,80
7250	437	3 – 10	1,7	2003 – 1962	61,11
7250	437	10 – 17	1,7	1962 – 1921	42,34
7250	437	17 – 23	1,7	1921 – 1886	38,41
7249	585	0 – 1	1,7	2021 – 2015	70,50
7249	585	1 – 3	1,7	2015 – 2003	71,00
7249	585	3 – 10	1,7	2003 – 1962	76,78
7249	585	10 – 20	1,7	1962 – 1903	56,55
7249	585	20 – 30	1,7	1903 – 1845	44,23
7222	320	0 – 1	1,7	2021 – 2015	58,98
7222	320	1 – 6	1,7	2015 – 1986	59,95
7222	320	6 – 12	1,7	1986 – 1950	49,05
7222	320	12 – 14	1,7	1950 – 1880	44,91
7222	320	24 – 32	1,7	1880 – 1833	42,22
7222	320	32 – 37	1,7	1833 – 1803	43,56
7198	18	0 – 0,5	8,9	2021 – 2020	11,60
7198	18	0,5 – 5	8,9	2020 – 2015	21,69
7198	18	5 - 7	8,9	2015 – 2013	17,10

It must be emphasised that the sedimentation rates from Table 5.2 are not calculated from the sediment samples themselves, and that it does not give an accurate or precise image of mercury burial in these sediments. The depth of the core samples that provided the calculated sedimentation rates are 13 meters for the 8,9 mm/years and 157 meters for the 1,7 mm/years (Rusakov, Borisov and Solovieva, 2019). Station 7253 is shallower than the sampling site used to calculate the sedimentation rate, and stations 7250, 7249 and 7222 are more than twice as deep and likely have different conditions, thus providing a rather big uncertainty for the dating of sediments in Table 5.2. However, the age of the sediments is plotted with the mercury concentration and shown in Figure 5.1.
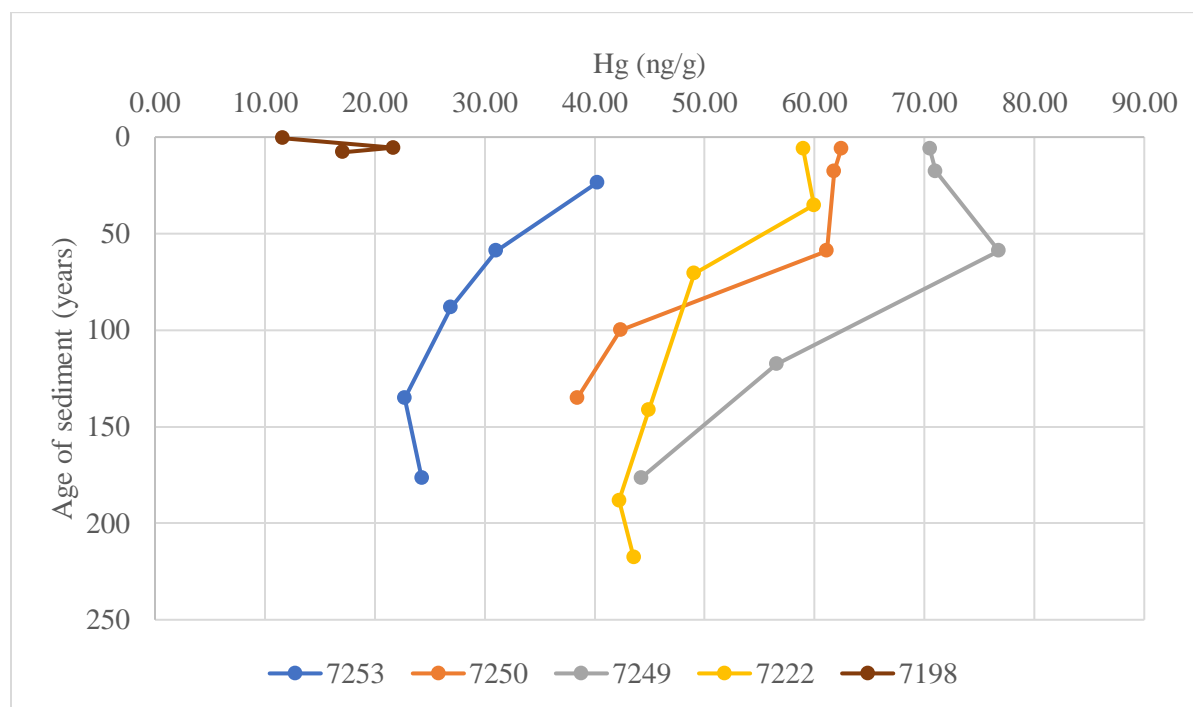
Figure 5.1: Graphic representation of the depth profile converted to the age of the sediment cores. The y-axis shows the age of the sediment core sample, and the x-axis show the concentration. The different colours represent the different sampling locations, and each station is given at the bottom of the graph.

The core samples from station 7222 and 7249 show decreasing amounts of mercury from the first to the second (and third for 7249) core depth, and core samples from station 7250 show a slower increase in the last 50-60 years than for the older sediments. If the dating is somewhat correct, this could be explained by decreasing amounts of elemental mercury in the atmosphere over the last 30 years (Zhang *et al.*, 2016) and reduction in the use of mercury in many areas (Beckers and Rinklebe, 2017). However, Zhang *et al.* (2016) point out that their findings on decreasing elemental mercury in the atmosphere are "inconsistent with current global emission inventories indicating flat or increasing emissions over that period". In addition, other studies have found that THg emissions have risen in recent years (AMAP, 2021). An increase of THg

from the surface layer to the next uppermost layers of the sediment cores applies to six of the measured core samples (Figure 4.1), where three of these six cores show a general trend using linear regression of decreasing concentrations with depth when the entire depth profile of the core is included.

Observed sedimentation rates from the arctic range from 0.0025–0.05 mm/year for the central Arctic Ocean and 0.1–2.5 mm/year for the shelf (Tesán Onrubia *et al.*, 2020). General estimations of the sedimentation rates in the Arctic Ocean are 0.03 mm/year, and for the open ocean and outer shelf 0.3 mm/year (Tesán Onrubia *et al.*, 2020). Using this estimation on sedimentation rates instead of the ones used in Table 5.1, the age of the bottom sediments will be significantly older. For instance, the bottom sediment from core sample 7222 would be between 12 300 years (using 0,03 mm/year) and 1 230 years (using 0,3 mm/year) instead of 248 years which Table 5.2 indicates. Going back to the question of whether the Hg concentration in the sediment layers below 10 cm can be considered natural background concentrations. Using the maximum sedimentation rate of 1,7 mm/year and 8,9 mm/year, the sediments at 10 cm depth would have accumulated 60 years ago, and using the minimum rate of 0,03 mm/year it would be over 3 000 years old. Given the uncertainties concerning the sedimentation rates, it is difficult to provide information regarding the dating of the different core depths and the exact source of the deposited mercury. Consequently, the trend of the cores will be the main argument for evaluating the sediment cores.

5.2.2 Vertical Distribution of Hg in Sediments

One study in the Arctic from 1999 analysed seven sediment core samples from the surface and down to 10 cm depth (Gobeil, Macdonald and Smith, 1999). They found the concentrations of five cores to decrease with depth, from 34 – 116 ng/g at the sediment surface to 10 – 65 ng/g at 5 cm depth and then remaining almost constant to 10 cm depth. In the last two cores, they found that the Hg decrease with depth was interrupted by a maximum (96 − 107 ng/g) at 7 − 8 cm (Gobeil, Macdonald and Smith, 1999). This study measured the concentration from each cm down in the sediment, in contrasts to the sample collection for this study, where there is little consistency in the depth intervals of the core samples. It can be argued that more consistent depth intervals would provide a more nuanced picture of the vertical distribution of mercury in sediments. The concentration span of the surface sediments from Gobeil *et al.* (1999) studies is slightly higher than for the ten cores in this thesis (11,60 ng/g – 70,50 ng/g). However, the same maximum concentration that interrupts the decrease with depth can be observed in the cores from stations 7249, 7222, and 7194 at respectively, 7.5 cm, 3.5 cm, and 6.5 cm when the middle of the depth interval is used (Figure 4.1).

Gobeil *et al.* (1999) explain the observed sediment profiles of mercury in their study with four distinct processes. These include textural changes in sedimentation particles or variations in Hg

input, decreasing sedimentation rate with no change in the flux of mercury, biomixing that can redistribute recently deposited mercury into deeper layers of the sediment, and diagenesis where redox-mediated reactions can redistribute mercury (Gobeil, Macdonald and Smith, 1999). If the sedimentation rate has decreased and the flux of mercury is constant, this would produce mercury sediment profiles that increase in concentration towards the surface (Gobeil, Macdonald and Smith, 1999). However, Gobeil *et al.* (1999) point out that this is unlikely as the sedimentation rate would have to decrease everywhere throughout the basins, and this is a phenomenon that has not been observed in previous studies. Hence, the increasing trend of mercury in the sediment cores in this thesis are likely to reflect an increase in the flux of mercury and not a decrease of the sedimentation rate itself. At the same time, elements in bottom sediment layers are thought to be redistributed by diagenesis processes (Aksentov *et al.*, 2021), and to further investigate if Hg has been recycled with other metals, the samples should be analysed for other trace metals, specially Mn and Fe, and correlations should be investigated.

It could be interesting to compare these sediment cores with cores from lower latitudes to evaluate if this increase has its origin in permafrost thawing. A study done in 2009 looked at sediment cores from lakes in the Canadian Arctic, Subarctic, and midlatitudes and found that there was a general increase in Hg concentrations in almost all cores (Muir *et al.*, 2009). They found that anthropogenic mercury deposition flux in lake sediments has increased significantly in the Arctic since the 1960s and in the midlatitudes since 1900 (Muir *et al.*, 2009). Other studies from lower latitudes have found no significant trend in the concentration of THg in sediment cores (Feng *et al.*, 2010; Orani *et al.*, 2019). A study from Ghana done in 2016 showed THg concentrations increasing with depth ranging from $18 \pm 5 - 25 \pm 5$ ng/g, and found that there was a marginal decline in Hg concentrations over the past two decades, while other metals showed increasing trends (Hogarh *et al.*, 2016). A study of sediment cores from Brazil found THg concentrations ranging between 15 and 44 ng/g and found a general tendency of Hg concentrations decreasing with depth (Sanders *et al.*, 2006). In the presented studies, only one found a decline in mercury accumulation in sediments. This study concluded that the cause of the marginal decline was processes that integrates Hg recovery in small-scale mining nearby, that limited the direct escape of Hg into the environment (Hogarh *et al.*, 2016). The fact that most of the sediment cores analysed in this thesis show increasing Hg concentration in the top layers of the sediment could indicate an increasing burial of mercury in the arctic, and it could be that mercury release from permafrost thawing is causing this. Still, it is important to note that atmospheric deposition in the Arctic has sources of emission from lower latitudes due to the long-range transport of pollutants, and a definite source of increasing mercury in the sediments is difficult to pinpoint. Especially as other studies from lower latitudes have also found increasing trends of THg in sediment cores.

5.3 Sediment Surface samples

When looking at the results of the sediment surface samples, it is important to realize that the presented concentration of Hg is only a snapshot of the true conditions in the Arctic sediment surfaces. Figures 4.5 and 4.6 show the distribution of mercury in the surface sediments in the sampling area. The red dots from Figure 4.5 indicate the samples with the highest concentration, and stations 7249, 7250, 6975, 6973 and 6966 have the highest concentrations of THg, all exceeding 60 ng/g Hg. Figures 4.7 – 4.9 focuses on each sea from Figure 4.5. As shown in Table 4.1 the average Hg concentrations from the surface sediments were higher in 2021 than in 2020, but as the samples from 2021 and 2020 are from different locations and have fewer sediment surface samples it does not provide information on the mercury accumulation rate in sediments. Based on the Norwegian system for classification of environmental quality of marine sediments (Figure 2.4) , most of the sediment samples would be classified as "Background levels" of mercury, and none of the samples exceeds "Good", which is described as having "No toxic effects" (Miljødirektoratet, 2020).

5.3.1 Depth of the Water Column

Figures 4.10 – 4.12 show the bottom surface sediment concentration of Hg plotted against the depth of the water column. It is difficult to conclude on a general trend as most samples are taken from shallower depths. However, if samples taken from 2021 are isolated (Figure 4.11), it may look like the concentration of Hg increases with an increasing depth of the water column. This correlates well with Dastoor *et al.* (2022) findings that Hg concentrations are higher in the deep basin than in shelf sediments. As the sedimentation rate is lower in the deep basin sediments, the burial of deposited mercury will happen at a slower rate than for the shelf sediments (Gobeil, Macdonald and Smith, 1999), hence the bottom surface sediments could have higher concentrations of total mercury compared with shelf sediments.

Dastoor *et al.* (2022) found the average Hg concentrations in surface sediments in the Arctic to be 60.4 ± 44.5 ng/g in the deep basin and 28.9 ± 22.0 ng/g in the shelf sediments. The deep basin is defined as surface sediments below 500 m depth. Of the analysed sediment samples, only one sample was taken from a water column depth exceeding 500 m. This is from station 7249, and it is the sample with the highest Hg concentration of 70,52 ng/g. This is within Dastoor et al.'s (2022) average concentration range. Other studies define the shelf from lower depths than 100 m (Kim, J. *et al.*, 2020). The average Hg concentration for all samples taken from depths below 100 m is 37,06 ng/g, and the average for all samples above 100 m depth is 38,60 ng/g, indicating that there is little difference. However, the shelf in the Arctic is shallow. For instance, the shelf of the East Siberian Sea has an average depth of 20 – 30 m (Dmitrenko *et al.*, 2010).

5.3.3 The Kara Sea

For the samples in the Kara Sea the average mercury concentration from all samples is 35,56 ng/g Hg, with concentrations ranging from 1,98 ng/g (Station 7011) to 70,50 ng/g Hg (Station 7249). The samples from the Kara Sea contains samples taken from 2020 and 2021. As Figure 4.7 shows, the surface sediments with the highest Hg concentration lie northeast of the island Novaya Zemlya. As mentioned, this island is experiencing surface melting due to seasonal changes (Melkonian *et al.*, 2016). This, together with these sampling locations having the deepest water columns could be the cause of the increasing amount of Hg concentration at this site.

The sample that are closest to the outlet of the Yenisey river (station 7194) show elevated Hg concentrations at 58,00 ng/g. The samples that are in the closest proximity to station 7194 do not show elevated concentrations. However, sampling station 7194 is a great distance from the outlet of the river and lies at the tip of a fjord. The sample lying closest to the outlet of the Ob River (station 7198) does not show elevated mercury concentrations (11,61 ng/g Hg). This sampling location also lies at the tip of a fjord and far away from the actual outlet of the river. Both the Yenisey and the Ob River are considered to be rivers of low runoff (Lim *et al.*, 2019), hence, the THg concentration at stations 7198 and 7194 are expected to be lower than for stations close to rivers of high runoff, like the Lena river.

Another study from 2001 did several measurements of Hg in the Kara Sea and found the average Hg concentration to range from 31 ± 12 ng/g (Sericano *et al.*, 2001). The calculated average concentration from the samples in this thesis are within this range. This could imply that the concentration of THg has not increased a significant amount within the last 20 years. However, Sericano's *et al.* (2001) study did not specify the exact concentrations measured at each location, giving little basis for comparison.

5.3.2 The Laptev Sea

For the samples in the Laptev Sea the average mercury concentration from all samples is 35,28 ng/g Hg, with mercury concentration ranging from 9,41 ng/g (Station 6943) to 68,42 ng/g (Station 6975). Figure 4.8 shows the Hg concentration for all samples in the Laptev Sea. For the mid part of the Laptev Sea (Figure A.1 in Appendix A) the concentration is relatively low, as is shown in Figure 4.8.

The river Lena has its outlet into the Laptev Sea, and the main channels for the annual Lena River freshwater and sediment discharge are covered by sampling stations 6973 – 6979. These stations are then followed by 6981, 6983, 6984, and 6985 in a consecutive straight line. Elevated mercury concentrations can be observed at station 6973 (63,67 ng/g), 6974 (57,61 ng/g), 6975 (68,42 ng/g), 6976 (50,60 ng/g), 6977 (53,92 ng/g) and 6978 (55,97 ng/g). This is consistent with

the Lena River being the largest annual Hg flux of all Arctic Rivers (Zolkos *et al.*, 2020). The next sampling station in the line is 6979, and this sample has a relatively low Hg concentration at 11,82 ng/g. This could indicate that runoff from the Lena River does not affect the composition of deposits after this point. However, the samples that follows station 6979 have slightly higher concentrations. If permafrost thawing contributes to elevated mercury levels in the sediments, it is expected to observe higher concentrations at these locations compared with earlier years. Liem-Nguyen *et al.* (2022) studied mercury in sediment samples sampled in 2008 close to the main channels for the river discharge of the Lena River and found concentrations of THg to range from 66,76 – 213,62 ng/g. The sampling locations from this study are taken from approximately the same locations as the sampling station 6973 – 6979 in this study, although the depth of the water column is lower, ranging from 6 – 23 m, whereas station 6973 – 6979 ranges from 12 – 25 m (Liem-Nguyen *et al.*, 2022). Indicating that the concentrations were higher for the samples taken in 2008 than the samples presented in this thesis. However, the proximity to the outlets of Lena River will impact the sediments, as can be seen by the reduction in THg from sample location 6978 to 6979, thus, if the samples had been taken in closer proximity by the shallower depths, we might have seen elevated concentrations.

5.3.4 The East Siberian Sea

For the samples in the East Siberian Sea the average mercury concentration from all the samples is 48,28 ng/g Hg, with mercury concentration ranging from 20,86 ng/g (Station 6968) to 67,13 ng/g (Station 6966). This is the highest average mercury concentration of all three seas, but this is also the sea with fewest sample locations. Figure 4.9 show that the samples taken near the shore have lower THg concentration than the samples taken further away from the shore. Stations 6961, 6962, 6963, 6964, and 6965 lies within the Trans Polar Drift (TPD), and the elevated concentrations in the centre of the East Siberian Sea could be explained by the TPD (Charette *et al.*, 2020). The TPD could have brought sedimentary material with glacier meltwater and transported it to the open sea. However, they could also be explained by the increasing depth of the water column.

The presented results do not deviate much from findings in other studies of surface sediments in the same area. A study from the East Siberian Sea found that THg concentrations were 55 ± 1, 61 ± 1, and 73 ± 1 ng/g at depths below 100 m, and increased with increasing depths to 97 ± 2 and 82 ± 2 ng/g at depths between 100 and 500 m (Kim, J. *et al.*, 2020). The sampling location that measured 55 ± 1 ng/g Hg was taken from 49 m depth and is near the following stations from this study 6961, 6962, 6963, 6964, and 6965, where the measured Hg concentration ranges between 54,76 – 57,56 ng/g and the depth ranges from 25 – 46 m. Thus, indicating that the measured Hg concentrations in this thesis are relatively correct compared to findings in other studies.

5.3.5 Distribution of Hg in Surface Sediments

If permafrost contributes to increasing mercury levels in sediments, the samples taken from locations near river outlets are expected to have increased THg concentrations. However, the distribution of mercury in the surface sediments from this study do not show a specific trend with increased mercury levels surrounding all major river outlets. Meaning that other factors are contributing significantly to the distribution of mercury in sediments. Among these factors are diageneses processes, the grain size of the sediments, the organic carbon content, the depth of the water column, and the amount of sunlight and biological activity (Dastoor *et al.*, 2022). As the sample locations are spread over a vast area, it is hard to pinpoint the contribution of mercury input in sediments from each isolated factor. Hence, there is a need for further research to establish if mercury deposition is changing over time. Observed changes over time can help conclude whether permafrost thawing contributes to elevated levels of mercury.

5.4 Further Work

This study illustrates the distribution of total mercury in Arctic sediments and the vertical distribution in sediment cores from the Kara Sea. However, this study does not provide knowledge on the speciation of mercury components or the mercury burial flux in sediments. For further work on these samples, several steps can be done to provide more information and give a broader understanding of the condition in the Arctic sediments. First, the concentration of ^{210}Pb in the core samples should be analysed so that the sedimentation rate can be calculated from each core station. This would provide information on the mercury burial rate in sediments and give a more precise dating from each sediment core interval. The grain size of each sediment sample should be analysed, as grain size will affect the sorption capacity of the sediment and consequently, the concentrations of trace elements (Budko *et al.*, 2022). In addition, correlations between the content of organic carbon and other trace elements, especially Mn and Fe. As the organic carbon is the main vector for transport of terrestrial Hg through riverine systems, and this could give information on where the mercury was transported from (Liem-Nguyen *et al.*, 2022). Correlations with Mn and Fe could indicate whether Hg has been recycled with other metals and is influenced by diagenesis processes (Aksentov *et al.*, 2021). Lastly, it would be interesting to investigate how much of the THg is present as MeHg. Mercury can be mobilized by methylation in sediments, and MeHg is bioavailable (Manahan, 2017). Knowing the amount of MeHg will provide important information on how much of the mercury in Arctic sediments that can be expected to accumulate in the food chain.

In future studies on mercury in marine Arctic sediments it could be useful to study the amount of mercury in the water column as well, since mercury tend to recycle in the upper stratified layer (Douglas *et al.*, 2012). However, the most important factor for establishing whether permafrost is

contributing to increased levels of Hg in sediments, is to observe changes in mercury deposition over time. This substantiates the need for further investigation of mercury in Arctic sediments.

6 Conclusion

This project aimed to investigate if the thawing of permafrost will contribute to elevated levels of mercury in Arctic sediments. Sediment cores showing increasing Hg concentrations in the top layers could indicate that deposition of mercury in sediments is increasing (Aksentov *et al.*, 2021). Another indication is elevated Hg concentrations surrounding river outlets, as a significant amount of mercury in river runoff comes from permafrost thawing (Douglas *et al.*, 2012; Schuster *et al.*, 2018; Dastoor *et al.*, 2022).

The total mercury (THg) concentration has been determined from 60 surface sediment samples from the Kara Sea, the Laptev Sea, the East Siberian Sea, and ten core sediment samples from the Kara Sea. The sampling of the core sediment samples took place in October 2021, and the sampling of the surface sediment samples was sampled in October 2020. Concentrations of THg from the surface sediments ranged from 1,99 ng/g to 70,52 ng/g, and the average for the Kara Sea, The Laptev Sea, and the East Siberian Sea were 35,56 ng/g, 35,28 ng/g, and 48,28 ng/g, respectively. The range in concentration for the Kara Sea, The Laptev Sea, and the East Siberian Sea were from 1,98 ng/g to 70,50 ng/g, 9,41 ng/g to 68,42 ng/g, and 20,86 ng/g to 67,13, respectively. Elevated levels of mercury were observed near Novaya Zemlya and near the outlet from the Lena River. This suggests that the spatial distribution of Hg is influenced by hydrodynamic sorting of riverine-derived material and the melting of glaciers.

The mercury concentration in the sediment cores ranged from 11,60 ng/g to 76,79 ng/g. The core samples analysed in this study show a general tendency of decreasing concentrations with increasing sediment depth, and seven of the ten cores show higher Hg concentration in the surface layer than in the deepest sediment interval. This could indicate that mercury accumulates in sediments at a higher rate than in previous years.

The reported mercury concentrations from this study are within the ranges of and comparable to previous studies from the Arctic Ocean (Aksentov *et al.*, 2021; Gobeil, Macdonald and Smith, 1999; Kim, J. *et al.*, 2020; Liem-Nguyen *et al.*, 2022; Muir *et al.*, 2009; Sericano *et al.*, 2001). There is no clear evidence for permafrost thawing being the source of mercury in the sediments. However, the results support the need for further research on permafrost thawing being a source of releasing mercury into the Arctic.

7 References

Agather, A. M. *et al.* (2019) Distribution of mercury species in the Western Arctic Ocean (US GEOTRACES GN01), *Marine Chemistry*, 216, pp. 103686.

Aksentov, K. I. *et al.* (2021) Assessment of mercury levels in modern sediments of the East Siberian Sea, *Marine Pollution Bulletin*, 168, pp. 112426.

Alfred Wegener Institute, A. (2022) Ocean Data View User's Guide (vol. 2022). Germany. Available at: https://odv.awi.de/.

AMAP (2011) *AMAP assessment 2011 : mercury in the Arctic*. Oslo: Arctic Monitoring and Assessment Programme.

AMAP (2021) 2021 AMAP Mercury Assessment. Summary for Policy-makers, i (AMAP), A. M. a. A. P. (ed.). Tromsø, Norway.

Amos, H. M. *et al.* (2013) Legacy impacts of all-time anthropogenic emissions on the global mercury cycle, *Global biogeochemical cycles*, 27(2), pp. 410-421.

Bakke, T. *et al.* (2010) Development of sediment quality criteria in Norway, *Journal of Soils and Sediments*, 10(2), pp. 172-178.

Baldé, C. *et al.* (2020) The global e-waste monitor–2020, United Nations University (UNU), *International Telecommunication Union (ITU) & International Solid Waste Association (ISWA), Bonn/Geneva/Vienna*. Available at: https://www.itu.int/en/ITU-D/Environment/Documents/Toolbox/GEM_2020_def.pdf.

Batley, G. (1999) Quality assurance in environmental monitoring, *Marine Pollution Bulletin*, 39(1-12), pp. 23-31.

Beckers, F. and Rinklebe, J. (2017) Cycling of mercury in the environment: Sources, fate, and human health implications: A review, *Critical Reviews in Environmental Science and Technology*, 47(9), pp. 693-794. doi: 10.1080/10643389.2017.1326277.

Britannica, T. E. o. E. (2012) *Laptev Sea, Encyclopedia Britannica*. Available at: https://www.britannica.com/place/Laptev-Sea (Accessed: 23.03.2022 2022).

Britannica, T. E. o. E. (2014) *Kara Sea, Encyclopedia Britannica*. Available at: https://www.britannica.com/place/Kara-Sea (Accessed: 23.03.2022 2022).

Britannica, T. E. o. E. (2021) *Mercury, Encyclopedia Britannica*. Available at: https://www.britannica.com/science/mercury-chemical-element (Accessed: 09.03.2022 2022).

Budko, D. F. *et al.* (2022) The Features of Distribution of Chemical Elements, including Heavy Metals and Cs-137, in Surface Sediments of the Barents, Kara, Laptev and East Siberian Seas, *Minerals*, 12(3), pp. 328.

Calder, R. S., Bromage, S. and Sunderland, E. M. (2019) Risk tradeoffs associated with traditional food advisories for Labrador Inuit, *Environmental research*, 168, pp. 496-506.

Carignan, J. and Sonke, J. (2010) The effect of atmospheric mercury depletion events on the net deposition flux around Hudson Bay, Canada, *Atmospheric Environment*, 44(35), pp. 4372-4379.

Cauwet, G. (1987) Influence of sedimentological features on the distribution of trace metals in marine sediments, *Marine Chemistry*, 22(2-4), pp. 221-234.

Chadburn, S. E. *et al.* (2017) An observation-based constraint on permafrost loss as a function of global warming, *Nature Climate Change*, 7(5), pp. 340-344. doi: 10.1038/nclimate3262.

Charette, M. A. *et al.* (2020) The transpolar drift as a source of riverine and shelf-derived trace elements to the central Arctic ocean, *Journal of Geophysical Research: Oceans*, 125(5), pp. e2019JC015920.

Chen, Y. *et al.* (2014) Global mercury emissions from combustion in light of international fuel trading, *Environmental science & technology*, 48(3), pp. 1727-1735.

Coulibaly, M. *et al.* (2016) Some aspects of speciation and reactivity of mercury in various matrices, *Comptes Rendus Chimie*, 19(7), pp. 832-840.

Crosby, N. T. and Prichard, E. (1995) *Quality in the analytical chemistry laboratory*. John Wiley & Sons.

Dastoor, A. *et al.* (2022) Arctic mercury cycling, *Nature Reviews Earth & Environment*, pp. 1-17.

Decharat, S. (2018) Urinary mercury levels among workers in E-waste shops in Nakhon Si Thammarat Province, Thailand, *Journal of Preventive Medicine and Public Health*, 51(4), pp. 196.

Dmitrenko, I. A. *et al.* (2010) Impact of the Arctic Ocean Atlantic water layer on Siberian shelf hydrography, *Journal of Geophysical Research: Oceans*, 115(C8).

Douglas, T. A. *et al.* (2012) The fate of mercury in Arctic terrestrial and aquatic ecosystems, a review, *Environmental Chemistry*, 9(4), pp. 321-355.

Driscoll, C. T. *et al.* (2013) Mercury as a global pollutant: sources, pathways, and effects, *Environmental science & technology*, 47(10), pp. 4967-4983.

El Houssainy, A. *et al.* (2020) Distribution and diagenesis of trace metals in marine sediments of a coastal Mediterranean area: St Georges Bay (Lebanon), *Marine Pollution Bulletin*, 155, pp. 111066.

EPA., U. S. (1998) Method 7473 *Mercury in solids and solutions by thermal decomposition, amalgamation, and atomic absorption spectrophotometry*. Washington DC.

Feng, X. *et al.* (2010) Tracing mercury contamination sources in sediments using mercury isotope compositions, *Environmental science & technology*, 44(9), pp. 3363-3368.

Ferrari, C. P. *et al.* (2008) Atmospheric mercury depletion event study in Ny-Alesund (Svalbard) in spring 2005. Deposition and transformation of Hg in surface snow during springtime, *Science of the total environment*, 397(1-3), pp. 167-177.

Fifield, F. W. and Haines, P. J. (2000) *Environmental analytical chemistry*. 2nd edn. Oxford: Blackwell Science.

Fisher, J. A. *et al.* (2013) Factors driving mercury variability in the Arctic atmosphere and ocean over the past 30 years, *Global biogeochemical cycles*, 27(4), pp. 1226-1235.

Galappaththi, H. K. and Suraweera, I. (2020) Risk of Mercury exposure during childhood: a review of Sri Lankan situation, *Reviews on Environmental Health*, 35(3), pp. 229-232.

Gobeil, C., Macdonald, R. W. and Smith, J. N. (1999) Mercury profiles in sediments of the Arctic Ocean basins, *Environmental science & technology*, 33(23), pp. 4194-4198.

Gueu, A., Ouffoué, S. K. and Digbéhi, B. Z. (2021) Mercury Concentration profile in sediment cores of a tropical lagoon under high anthropogenic activities around an Urban City—Abidjan, Côte d'Ivoire, *Journal of Geoscience and Environment Protection*, 9(5), pp. 83-94.

Gunnarsson, B. (2021) Recent ship traffic and developing shipping trends on the Northern Sea Route—Policy implications for future arctic shipping, *Marine Policy*, 124, pp. 104369.

Gunnarsson, B. and Moe, A. (2021) Ten years of international shipping on the Northern Sea Route: trends and challenges.

Gworek, B. *et al.* (2017) Air contamination by mercury, emissions and transformations—a review, *Water, Air, & Soil Pollution*, 228(4), pp. 1-31.

Hogarh, J. N. *et al.* (2016) Contamination from mercury and other heavy metals in a mining district in Ghana: discerning recent trends from sediment core analysis, *Environmental Systems Research*, 5(1), pp. 1-9.

Hsu-Kim, H. *et al.* (2013) Mechanisms regulating mercury bioavailability for methylating microorganisms in the aquatic environment: a critical review, *Environmental science & technology*, 47(6), pp. 2441-2456.

IRMM, I. f. R. M. a. M. (2007) CERTIFIED REFERENCE MATERIAL BCR– 277R, CERTIFICATE OF ANALYSIS Belgium: European Comission, Joint research centre.

ISO (2004) ISO 5667-19:2004, Water quality - Sampling - Part 19: Guidance on sampling in marine sediments Available at: https://www.standard.no/no/Nettbutikk/produktkatalogen/Produktpresentasjon/?ProductID=145057.

Kim, H. *et al.* (2020) Dietary mercury intake and colorectal cancer risk: A case-control study, *Clinical Nutrition*, 39(7), pp. 2106-2113.

Kim, J. *et al.* (2020) Mass budget of methylmercury in the East Siberian Sea: the importance of sediment sources, *Environmental science & technology*, 54(16), pp. 9949-9957.

Koven, C. D., Riley, W. J. and Stern, A. (2013) Analysis of permafrost thermal dynamics and response to climate change in the CMIP5 Earth System Models, *Journal of Climate*, 26(6), pp. 1877-1900.

Li, W. C. and Tse, H. F. (2015) Health risk and significance of mercury in the environment, *Environmental Science and Pollution Research*, 22(1), pp. 192-201. doi: 10.1007/s11356-014-3544-x.

Lian, P. *et al.* (2021) Mechanistic investigation of dimethylmercury formation mediated by a sulfide mineral surface, *The Journal of Physical Chemistry A*, 125(24), pp. 5397-5405.

Libes, S. (2011) *Introduction to marine biogeochemistry*. Academic Press.

Liem-Nguyen, V. *et al.* (2022) Spatial patterns and distributional controls of total and methylated mercury off the Lena River in the Laptev Sea sediments, *Marine Chemistry*, 238, pp. 104052.

Lilleøren, K. (2021) *permafrost*. Available at: https://snl.no/permafrost (Accessed: 09.03.2022 2022).

Lim, A. G. *et al.* (2019) Enhanced particulate Hg export at the permafrost boundary, western Siberia, *Environmental Pollution*, 254, pp. 113083.

Lim, A. G. *et al.* (2020) A revised pan-Arctic permafrost soil Hg pool based on Western Siberian peat Hg and carbon observations, *Biogeosciences*, 17(12), pp. 3083-3097.

Liu, L. *et al.* (2019) Vertical distributions of mercury in marine sediment cores from central and southern part of Bohai Sea, China, *Ecotoxicology and environmental safety*, 170, pp. 399-406.

MacDougall, D. and Crummett, W. B. (1980) Guidelines for data acquisition and data quality evaluation in environmental chemistry, *Analytical Chemistry*, 52(14), pp. 2242-2249.

Maggi, C. *et al.* (2009) Methylmercury determination in marine sediment and organisms by Direct Mercury Analyser, *Anal Chim Acta*, 641(1), pp. 32-36. doi: 10.1016/j.aca.2009.03.033.

Manahan, S. E. (2017) *Environmental Chemistry*. 10th edn. Baco Raton, Fla: CRC Press.

Mason, R. P. (2009) Mercury emissions from natural processes and their importance in the global mercury cycle *Mercury fate and transport in the global atmosphere.* Springer, pp. 173-191.

McClelland, J. W. *et al.* (2012) The Arctic ocean estuary, *Estuaries and Coasts*, 35(2), pp. 353-368.

Meador, J. P., Ernest, D. W. and Kagley, A. N. (2005) A comparison of the non-essential elements cadmium, mercury, and lead found in fish and sediment from Alaska and California, *Science of the total environment*, 339(1-3), pp. 189-205.

Melkonian, A. K. *et al.* (2016) Recent changes in glacier velocities and thinning at Novaya Zemlya, *Remote Sensing of Environment*, 174, pp. 244-257.

Meredith, M. *et al.* (2019) Polar Regions. Chapter 3, IPCC Special Report on the Ocean and Cryosphere in a Changing Climate.

Milestone-Srl (2022) *DMA-80 evo*. Available at: https://www.milestonesrl.com/products/mercury-determination/dma-80-evo (Accessed: 15.03.2022 2022).

Miljødirektoratet (2020) Grenseverdier for klassifisering av vann, sediment og biota.(Quality standards for water, sediment and biota), *Miljødirektoratet basert på bakgrunnsdata fra Aquateam, NIVA og NGI*. Available at: https://www.miljodirektoratet.no/globalassets/publikasjoner/M608/M608.pdf.

Morel, F. M. (2016) *Mechanisms of Hg (II) uptake and methylation in methylating bacteria*. Princeton Univ., NJ (United States).

Muir, D. *et al.* (2009) Spatial trends and historical deposition of mercury in eastern and northern Canada inferred from lake sediment cores, *Environmental science & technology*, 43(13), pp. 4802-4809.

NFR (2021) *BEST Siberian Project (NFR project 315317)*. Available at: https://sites.google.com/view/best-siberian/about-project (Accessed: 22.04.22 2022).

O'Connor, D. *et al.* (2019) Mercury speciation, transformation, and transportation in soils, atmospheric flux, and implications for risk management: A critical review, *Environment International*, 126, pp. 747-761.

Olli, K. *et al.* (2002) Seasonal variation in vertical flux of biogenic matter in the marginal ice zone and the central Barents Sea, *Journal of Marine Systems*, 38(1-2), pp. 189-204.

Orani, A. M. *et al.* (2019) First assessment on trace elements in sediment cores from Namibian coast and pollution sources evaluation, *Science of the total environment*, 669, pp. 668-682.

Overduin, P. P. *et al.* (2007) The evolution and degradation of coastal and offshore permafrost in the Laptev and East Siberian Seas during the last climatic cycle, *Coastline changes: interrelation of climate and geological processes*, 426, pp. 97-111.

Overland, J. *et al.* (2019) The urgency of Arctic change, *Polar Science*, 21, pp. 6-13.

Polyak, L. and Jakobsson, M. (2011) Quaternary Sedimentation in the Arctic Ocean: RECENT ADVANCES AND FURTHER CHALLENGES, *Oceanography (Washington, D.C.)*, 24(3), pp. 52-64. doi: 10.5670/oceanog.2011.55.

Rusakov, V. Y., Borisov, A. and Solovieva, G. Y. (2019) Sedimentation rates in different facies–genetic types of bottom sediments in the Kara Sea: evidence from the 210Pb and 137Cs radionuclides, *Geochemistry International*, 57(11), pp. 1185-1200.

Sanders, C. J. *et al.* (2006) Mercury flux to estuarine sediments, derived from Pb-210 and Cs-137 geochronologies (Guaratuba Bay, Brazil), *Marine Pollution Bulletin*, 52(9), pp. 1085-1089.

Sanei, H. *et al.* (2021) High mercury accumulation in deep-ocean hadal sediments, *Scientific reports*, 11(1), pp. 1-8.

Schaefer, J. K. *et al.* (2011) Active transport, substrate specificity, and methylation of Hg (II) in anaerobic bacteria, *Proceedings of the National Academy of Sciences*, 108(21), pp. 8714-8719.

Schaefer, K. *et al.* (2020) Potential impacts of mercury released from thawing permafrost, *Nature Communications*, 11(1), pp. 4650. doi: 10.1038/s41467-020-18398-5.

Schlüter, K. (2000) evaporation of mercury from soils. An integration and synthesis of current knowledge, *Environmental Geology*, 39(3), pp. 249-271.

Schuster, P. F. *et al.* (2018) Permafrost Stores a Globally Significant Amount of Mercury, *Geophysical Research Letters*, 45(3), pp. 1463-1471. doi: https://doi.org/10.1002/2017GL075571.

Schuur, E. A. *et al.* (2015) Climate change and the permafrost carbon feedback, *Nature*, 520(7546), pp. 171-179.

Sericano, J. L. *et al.* (2001) Trace contaminant concentrations in the Kara Sea and its adjacent rivers, Russia, *Marine Pollution Bulletin*, 42(11), pp. 1017-1030.

Shakhova, N. *et al.* (2017) Current rates and mechanisms of subsea permafrost degradation in the East Siberian Arctic Shelf, *Nature Communications*, 8(1), pp. 1-13.

Skov, H. *et al.* (2006) Fluxes of reactive gaseous mercury measured with a newly developed method using relaxed eddy accumulation, *Atmospheric Environment*, 40(28), pp. 5452-5463.

Soerensen, A. L. *et al.* (2016) A mass budget for mercury and methylmercury in the Arctic Ocean, *Global biogeochemical cycles*, 30(4), pp. 560-575.

Sunderland, E. M. and Mason, R. P. (2007) Human impacts on open ocean mercury concentrations, *Global biogeochemical cycles*, 21(4).

Sundseth, K. *et al.* (2017) Global sources and pathways of mercury in the context of human health, *International journal of environmental research and public health*, 14(1), pp. 105.

Tamashiro, H. *et al.* (1984) Causes of death in Minamata disease: analysis of death certificates, *International archives of occupational and environmental health*, 54(2), pp. 135-146.

Tesán Onrubia, J. A. *et al.* (2020) Mercury export flux in the Arctic Ocean estimated from 234Th/238U disequilibria, *ACS Earth and Space Chemistry*, 4(5), pp. 795-801.

UNEP, A. a. (2013) *Technical Background Report for the Global Mercury Assessment 2013*. AMAP and UNEP, Oslo and Geneva.

Wang, F., Pućko, M. and Stern, G. (2017) Transport and transformation of contaminants in sea ice, *Sea Ice*, pp. 472-491.

West, J. *et al.* (2020) Dimethylmercury degradation by dissolved sulfide and mackinawite, *Environmental science & technology*, 54(21), pp. 13731-13738.

WHO (2017) *Mercury and health*. Available at: https://www.who.int/news-room/fact-sheets/detail/mercury-and-health (Accessed: 09.03.2022 2022).

Wu, P. *et al.* (2021) Bottom-Heavy Trophic Pyramids Impair Methylmercury Biomagnification in the Marine Plankton Ecosystems, *Environmental science & technology*, 55(22), pp. 15476-15483.

Ye, B.-J. *et al.* (2016) Evaluation of mercury exposure level, clinical diagnosis and treatment for mercury intoxication, *Annals of Occupational and Environmental Medicine*, 28(1), pp. 1-8.

Yorifuji, T., Tsuda, T. and Harada, M. (2013) Minamata disease: a challenge for democracy and justice, *Late Lessons from Early Warnings: Science, Precaution, Innovation. Copenhagen, Denmark: European Environment Agency*.

Zhang, Y. *et al.* (2015) Biogeochemical drivers of the fate of riverine mercury discharged to the global and Arctic oceans, *Global biogeochemical cycles*, 29(6), pp. 854-864.

Zhang, Y. *et al.* (2016) Observed decrease in atmospheric mercury explained by global decline in anthropogenic emissions, *Proceedings of the National Academy of Sciences*, 113(3), pp. 526-531.

Zolkos, S. *et al.* (2020) Mercury export from Arctic great rivers, *Environmental science & technology*, 54(7), pp. 4140-4148.

Appendices

Appendix A: Sample Location

Appendix B: Sample Preparation

Appendix C: DMA-80 Analysis

Appendix A – Sample Location

Table A.1: Information regarding sampling location, sampling dates and depth of the water column. ND stands for "No Data".

Station	Location	Latitude	Longitude	Date	Depth (m)
7253	Kara Sea	76,025	73,003	23.10.2021	110
7250	Kara Sea	77,500	68,995	22.10.2021	437
7249	Kara Sea	77,000	70,002	22.10.2021	585
7247	Kara Sea	80,030	73,598	21.10.2021	ND
7222	Kara Sea	75,832	68,910	16.10.2021	320
7218	Kara Sea	74,915	69,722	16.10.2021	38
7212	Kara Sea	69,963	65,342	12.10.2021	37
7200	Kara Sea	71,848	67,198	11.10.2021	50
7198	Kara Sea	72,082	73,043	10.10.2021	18
7194	Kara Sea	73,168	79,873	08.10.2021	27,5
7192	Kara Sea	73,933	85,052	07.10.2021	21,5
7001	Kara Sea	78,092	104,632	23.10.2020	230
7006	Kara Sea	74,206	79,025	25.10.2020	32
7007	Kara Sea	73,866	79,286	26.10.2020	30
7008	Kara Sea	73,674	77,829	26.10.2020	21
7009	Kara Sea	73,768	76,820	26.10.2020	24
7010	Kara Sea	73,863	75,672	26.10.2020	21
7011	Kara Sea	73,958	74,533	26.10.2020	21
7012	Kara Sea	74,053	73,383	26.10.2020	30
6939	Laptev Sea	77,285	122,096	6.10.2020	294
6941	Laptev Sea	77,102	125,095	7.10.2020	362
6942	Laptev Sea	77,093	124,902	7.10.2020	178
6943	Laptev Sea	77,068	125,784	7.10.2020	204
6946	Laptev Sea	77,144	126,798	8.10.2020	3,2
6947	Laptev Sea	76,776	125,828	8.10.2020	72
6950	Laptev Sea	76,880	127,015	9.10.2020	72
6948	Laptev Sea	76,778	125,821	9.10.2020	72
6952	Laptev Sea	76,892	127,793	9.10.2020	63,8
6953	Laptev Sea	76,895	127,818	9.10.2020	64,6
6955	Laptev Sea	76,923	127,953	10.10.2020	65
6959	Laptev Sea	77,633	131,194	10.10.2020	72
6960	Laptev Sea	78,074	133,597	10.10.2020	208
6971	Laptev Sea	73,012	142,367	16.10.2020	12
6973	Laptev Sea	72,013	130,330	17.10.2020	16
6974	Laptev Sea	72,484	130,421	18.10.2020	12

6975	Laptev Sea	72,483	130,538	18.10.2020	14
6972	Laptev Sea	72,977	139,769	16.10.2020	14
6976	Laptev Sea	73,114	130,367	18.10.2020	25
6977	Laptev Sea	73,112	130,356	18.10.2020	22
6978	Laptev Sea	73,093	130,278	19.10.2020	21
6979	Laptev Sea	73,468	130,069	19.10.2020	21
6981	Laptev Sea	74,513	130,068	19.10.2020	34
6983	Laptev Sea	75,038	130,074	20.10.2020	40
6984	Laptev Sea	75,563	130,077	20.10.2020	49
6985	Laptev Sea	76,087	130,074	20.10.2020	31
6986	Laptev Sea	76,615	130,075	20.10.2020	62
6991	Laptev Sea	76,395	125,422	21.10.2020	51
6992	Laptev Sea	76,392	125,428	21.10.2020	52
6994	Laptev Sea	77,265	120,604	22.10.2020	260
6995	Laptev Sea	77,900	105,052	23.10.2020	224
6961	East Siberian Sea	74,992	160,980	13.10.2020	25
6962	East Siberian Sea	74,992	160,989	13.10.2020	45
6963	East Siberian Sea	74,913	160,947	13.10.2020	45
6964	East Siberian Sea	74,905	160,928	14.10.2020	45
6965	East Siberian Sea	74,904	160,941	14.10.2020	46
6966	East Siberian Sea	74,053	155,805	15.10.2020	42
6967	East Siberian Sea	73,460	153,773	15.10.2020	30
6968	East Siberian Sea	72,979	152,133	15.10.2020	15
6969	East Siberian Sea	72,500	150,495	15.10.2020	17
6970	East Siberian Sea	72,909	145,015	16.10.2020	12
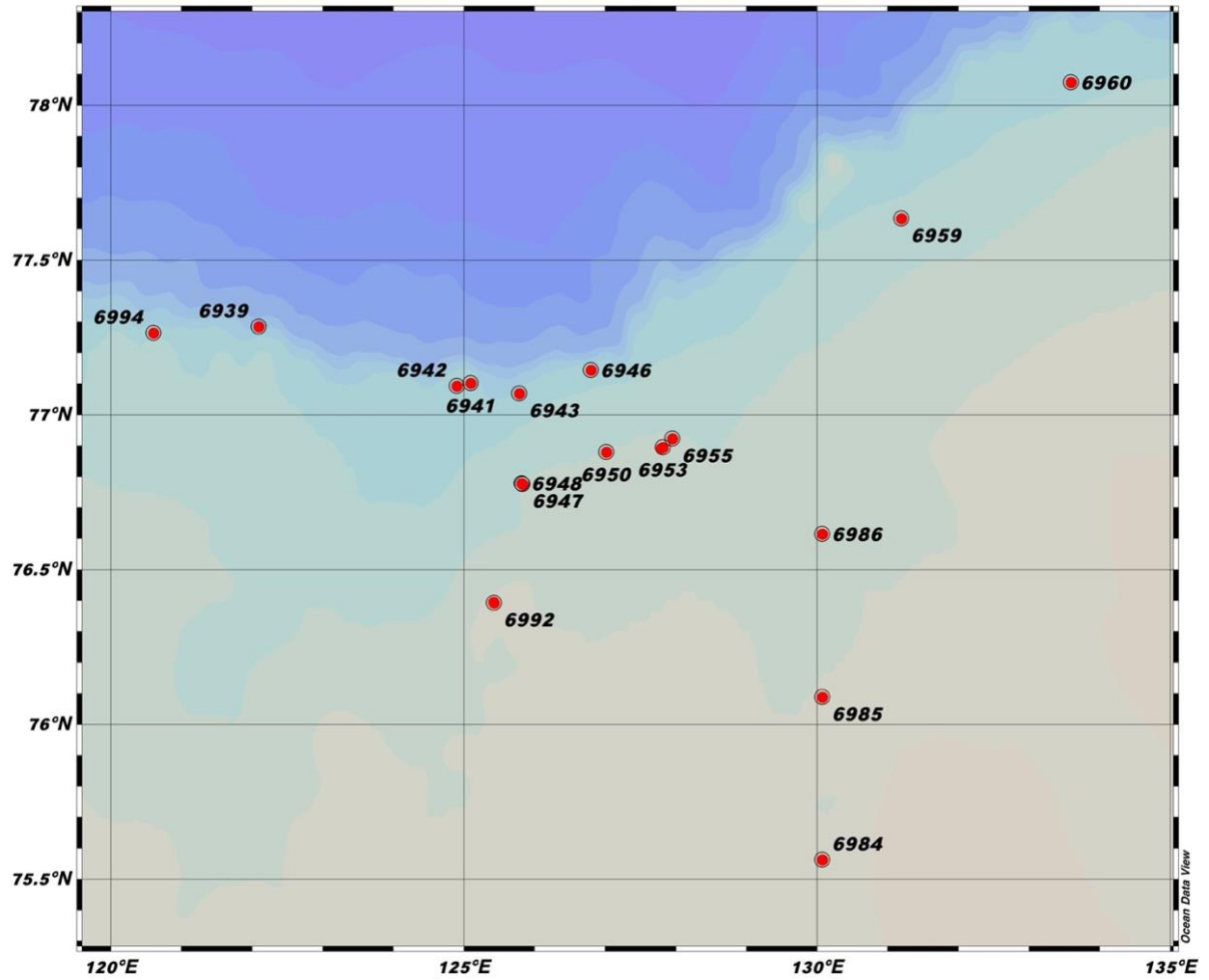
Figure A.1: A zoom in on Figure 3.5 from the Laptev Sea.

Appendix B – Sample Preparation

Table B.1: The weight of the samples from 2020 before and after freeze drying.

Station	Initial weight (g)	Final weight (g)
6939	30,33	13,96
6941	25,23	14,38
6942	24,22	16,11
6943	24,48	13,81
6946	19,76	10,63
6947	18,43	8,50
6950	12,90	7,36
6948	24,69	10,67
6952	32,24	14,14
6953	17,95	10,00
6955	16,16	5,14
6959	31,76	13,21
6960	31,08	13,45
6961	30,62	12,24
6962	36,36	14,97
6963	24,07	10,45
6964	15,03	5,91
6965	35,53	15,82
6966	13,81	4,78
6967	25,97	11,70
6968	47,36	31,18
6968	47,36	31,18
6968	47,36	31,18
6969	27,59	14,28
6970	53,89	25,94
6970	53,89	25,94
6970	53,89	25,94
6971	31,59	15,63
6973	23,05	8,03
6974	15,92	6,47
6975	29,96	12,04
6972	10,05	7,08
6976	37,76	16,45
6977	24,40	10,28
6978	16,95	6,71
6979	40,13	27,63

6981	32,61	12,70
6983	18,90	6,81
6984	13,42	4,78
6985	27,62	8,84
6986	37,11	12,40
6991	36,80	24,94
6992	32,32	20,23
6994	17,52	8,30
6995	25,86	11,26
7001	26,12	11,56
7006	12,56	3,99
7007	14,69	6,54
7008	20,24	15,81
7009	25,13	8,73
7010	37,91	29,87
7011	34,71	26,18
7012	9,82	3,64

Table B.2: The weight of the subsampled samples from 2021 before and after freeze drying.

Station	Depth interval (cm)	Initial weight (g)	Final weight (g)	Remarks
7253	0 - 4	17,87	6,78	
7253	4 - 10	10,25	4,57	Cracked lid
7253	10 - 15	11,22	6,26	Cracked lid
7253	15 - 23	14,07	7,74	Cracked lid
7253	23 - 30	13,07	7,47	Cracked lid
7250	0 - 1	12,03	3,94	
7250	1 - 3	12,02	5,09	Cracked lid
7250	3 - 10	13,80	6,37	
7250	10 - 17	11,41	6,26	
7250	17 - 23	11,50	6,25	
7249	0 - 1	11,29	3,35	Cracked lid
7249	1 - 3	8,71	2,64	
7249	3 - 10	8,36	3,05	Cracked lid
7249	10 - 20	10,12	4,66	
7249	20 - 30	8,39	3,96	Cracked lid
7247	ND	19,11	11,20	
7222	0 - 1	10,41	3,09	
7222	1 - 6	15,58	5,54	
7222	6 - 12	15,94	6,48	

7222	12 - 24	16,79	6,95	
7222	24 - 32	17,27	6,82	
7222	32 - 37	17,20	6,83	
7247	ND	19,11	11,20	
7218	0 - 0,5	20,58	10,22	
7218	0,5 - 2,5	20,12	12,30	
7218	2,5 - 5	15,93	10,22	
7218	5 - 10	17,23	11,45	
7212	0 - 5	23,74	13,97	
7212	5 - 10	20,80	12,68	
7212	10 - 14	16,57	11,79	
7200	0 - 1	13,21	5,77	
7200	1 - 3	13,47	6,06	
7200	3 - 5	12,37	7,10	
7200	5 - 7	11,92	6,66	
7200	7 - 11	14,52	8,02	
7198	0 - 0,5	0,55	0,33	
7198	0,5 - 5	18,95	10,52	
7198	5 - 7	15,12	9,38	
7194	0 - 2	18,80	5,49	
7194	2 - 5	16,29	5,07	
7194	5 - 10	15,71	6,15	
7194	10 - 20	15,36	6,58	Cracked lid
7194	20 - 30	14,34	5,98	Cracked lid
7192	0 - 1	16,82	7,10	
7192	1 - 2	16,61	8,25	
7192	2 - 10	19,53	9,24	
7192	10 - 17	18,92	10,19	
7192	17 - 26	21,96	12,07	

Appendix C – DMA-80 Analysis

The following tables show information from the DMA-80 analysis, including date of analysis, the amount of sample analysed, the absorbance cell that was used for quantification and its peak height, the total amount of Hg and the measured Hg concentration.

Table C.1: DMA-80 measurements for samples taken from station 7253

Depth (cm)	Date	Amount (g)	Absorbance cell	Peak Height	Hg (ng)	Concentration(ng/g)
0 - 4	09.02.2022	0,0509	0	0,2414	2,049	40,260
4 - 10	09.02.2022	0,0686	0	0,2504	2,130	31,055
10 - 15	09.02.2022	0,0732	0	0,2328	1,972	26,939
15 - 23	09.02.2022	0,0499	0	0,1369	1,135	22,738
23 - 30	09.02.2022	0,0602	0	0,1752	1,463	24,300
23 - 30	29.03.2022	0,0559	0	0,1611	1,332	23,825

Table C.2: DMA-80 measurements for samples taken from station 7250

Depth (cm)	Date	Amount (g)	Absorbance cell	Peak Height	Hg (ng)	Concentration(ng/g)
0 - 1	10.02.2022	0,0645	0	0,4509	4,029	62,457
1 - 3	09.02.2022	0,0888	0	0,5814	5,489	61,817
3 - 10	09.02.2022	0,0635	0	0,4333	3,882	61,127
10 - 17	09.02.2022	0,0607	0	0,2987	2,571	42,354
17 - 23	09.02.2022	0,0589	0	0,2653	2,263	38,425

Table C.3: DMA-80 measurements for samples taken from station 7249

Depth (cm)	Date	Amount (g)	Absorbance cell	Peak Height	Hg (ng)	Concentration(ng/g)
0 - 1	09.02.2022	0,0526	0	0,4163	3,709	70,515
1 - 3	09.02.2022	0,0523	0	0,4168	3,714	71,016
3 - 10	09.02.2022	0,0591	0	0,4961	4,539	76,795
10 - 20	09.02.2022	0,0471	0	0,3087	2,664	56,565
20 - 30	09.02.2022	0,1013	0	0,4908	4,482	44,245

Table C.4: DMA-80 measurements for the sample taken from station 7247.

Depth (cm)	Date	Amount (g)	Absorbance cell	Peak Height	Hg (ng)	Concentration(ng/g)
ND	10.02.2022	0,0539	0	0,1807	1,476	27,381
ND	29.03.2022	0,0506	0	0,1793	1,489	29,423
ND	29.03.2022	0,051	0	0,1854	1,542	30,231

Table C.5: DMA-80 measurements for samples taken from station 7222

Depth (cm)	Date	Amount (g)	Absorbance cell	Peak Height	Hg (ng)	Concentration(ng/g)
0 - 1	09.02.2022	0,0495	0	0,3358	2,920	58,995
1 - 6	10.02.2022	0,0571	0	0,3920	3,424	59,962
6 - 12	10.02.2022	0,0526	0	0,3046	2,581	49,065
12 - 24	10.02.2022	0,059	0	0,3121	2,651	44,931
24 - 32	10.02.2022	0,0507	0	0,2566	2,141	42,237
32 - 37	10.02.2022	0,0509	0	0,2651	2,218	43,578

Table C.6: DMA-80 measurements for samples taken from station 7218

Depth (cm)	Date	Amount (g)	Absorbance cell	Peak Height	Hg (ng)	Concentration(ng/g)
0 - 0,5	10.02.2022	0,0604	0	0,1611	1,309	21,675
0,5 - 2,5	10.02.2022	0,0511	0	0,1471	1,191	23,315
2,5 - 5	10.02.2022	0,0587	0	0,1888	1,545	26,325
5 - 10	10.02.2022	0,0595	0	0,1738	1,417	23,814

Table C.7: DMA-80 measurements for samples taken from station 7212

Depth (cm)	Date	Amount (g)	Absorbance cell	Peak Height	Hg (ng)	Concentration(ng/g)
0 - 5	10.02.2022	0,0523	0	0,1450	1,174	22,444
5 - 10	10.02.2022	0,0626	0	0,1776	1,449	23,152
10 - 14	10.02.2022	0,0539	0	0,1591	1,292	23,976

Table C.8: DMA-80 measurements for samples taken from station 7200

Depth (cm)	Date	Amount (g)	Absorbance cell	Peak Height	Hg (ng)	Concentration(ng/g)
0 - 1	10.02.2022	0,054	0	0,2198	1,814	33,600
1 - 3	10.02.2022	0,0632	0	0,2367	1,964	31,070
3 - 5	10.02.2022	0,0564	0	0,1969	1,615	28,636
5 - 7	10.02.2022	0,068	0	0,2340	1,940	28,525
7 - 11	10.02.2022	0,0636	0	0,2154	1,776	27,924

Table C.9: DMA-80 measurements for samples taken from station 7198

Depth (cm)	Date	Amount (g)	Absorbance cell	Peak Height	Hg (ng)	Concentration(ng/g)
0 - 0,5	14.02.2022	0,0459	0	0,0659	0,533	11,614
0,5 - 5	14.02.2022	0,051	0	0,1353	1,107	21,704
5 - 7	14.02.2022	0,0579	0	0,1215	0,991	17,117

Table C.10: DMA-80 measurements for samples taken from station 7194

Depth (cm)	Date	Amount (g)	Absorbance cell	Peak Height	Hg (ng)	Concentration(ng/g)
0 - 2	14.02.2022	0,0629	0	0,4115	3,649	58,014
2 - 5	14.02.2022	0,0503	0	0,3449	2,991	59,465
5 - 10	14.02.2022	0,0556	0	0,3992	3,525	63,399
10 - 20	14.02.2022	0,0535	0	0,2971	2,538	47,445
20 - 30	14.02.2022	0,0486	0	0,2457	2,068	42,546

Table C.11: DMA-80 measurements for samples taken from station 7192

Depth (cm)	Date	Amount (g)	Absorbance cell	Peak Height	Hg (ng)	Concentration(ng/g)
0 - 1	14.02.2022	0,0519	0	0,2408	2,024	38,995
1 - 2	14.02.2022	0,0591	0	0,2554	2,155	36,469
1 - 2	29.03.2022	0,0571	0	0,2384	2,010	35,206
1 - 2	29.03.2022	0,0566	0	0,2357	1,986	35,091
2 - 10	14.02.2022	0,0582	0	0,2400	2,017	34,651
10 - 17	14.02.2022	0,0662	0	0,2663	2,255	34,057
17 - 26	14.02.2022	0,0534	0	0,2001	1,663	31,142

Table C.12: DMA-80 measurements for samples taken in 2020

Station	Date	Amount (g)	Absorbance cell	Peak Height	Hg (ng)	Hg Concentration(ng/g)
6939	11.03.2022	0,0516	0	0,1372	1,126	21,816
6941	11.03.2022	0,0749	0	0,1612	1,330	17,754
6942	11.03.2022	0,0760	0	0,1148	0,938	12,338
6943	11.03.2022	0,0505	0	0,0586	0,476	9,423
6946	11.03.2022	0,0558	0	0,2171	1,816	32,547
6947	11.03.2022	0,0508	0	0,1765	1,461	28,766
6950	11.03.2022	0,0523	0	0,1662	1,373	26,245
6948	11.03.2022	0,0560	0	0,1814	1,504	26,851
6952	11.03.2022	0,0518	0	0,1215	0,994	19,183
6953	11.03.2022	0,0641	0	0,1111	0,907	14,148
6955	16.03.2022	0,0556	0	0,2818	2,401	43,189
6959	16.03.2022	0,0495	0	0,1951	1,623	32,794
6960	16.03.2022	0,0583	0	0,2266	1,901	32,610
6961	16.03.2022	0,0555	0	0,3648	3,189	57,464
6962	16.03.2022	0,0524	0	0,3440	2,988	57,012
6963	16.03.2022	0,0499	0	0,3216	2,773	55,578
6964	16.03.2022	0,0506	0	0,3214	2,772	54,775
6965	16.03.2022	0,0515	0	0,3417	2,965	57,579
6966	16.03.2022	0,0522	0	0,3967	3,505	67,143
6967	16.03.2022	0,0518	0	0,3058	2,625	50,668
6968	29.03.2022	0,0493	0	0,1257	1,031	20,915
6968	29.03.2022	0,0540	0	0,1358	1,116	20,672
6968	29.03.2022	0,0543	0	0,1389	1,142	21,039
6969	22.03.2022	0,0493	0	0,1509	1,245	25,257
6970	22.03.2022	0,0525	0	0,2306	1,940	36,958
6970	22.03.2022	0,0505	0	0,2221	1,865	36,922
6970	22.03.2022	0,0508	0	0,2186	1,834	36,092
6971	22.03.2022	0,0513	0	0,2290	1,926	37,544
6973	22.03.2022	0,0512	0	0,3716	3,261	63,686
6974	22.03.2022	0,0524	0	0,3469	3,020	57,627
6975	22.03.2022	0,0523	0	0,4036	3,580	68,441
6972	22.03.2022	0,0617	0	0,1026	0,839	13,600
6976	22.03.2022	0,0529	0	0,3110	2,678	50,614
6977	22.03.2022	0,0584	0	0,3603	3,150	53,936
6978	22.03.2022	0,0599	0	0,3810	3,354	55,985
6979	22.03.2022	0,0540	0	0,0784	0,639	11,839
6981	22.03.2022	0,0509	0	0,2307	1,941	38,134
6983	22.03.2022	0,0503	0	0,3084	2,653	52,744
6984	22.03.2022	0,0499	0	0,2879	2,462	49,331
6985	22.03.2022	0,0494	0	0,2784	2,374	48,050
6986	22.03.2022	0,0500	0	0,2582	2,189	43,780
6991	22.03.2022	0,0537	0	0,0725	0,591	11,013
6992	22.03.2022	0,0539	0	0,1199	0,983	18,243

6994	22.03.2022	0,0508	0	0,1819	1,512	29,757
6995	29.03.2022	0,0511	0	0,2872	2,456	48,058
7001	29.03.2022	0,0548	0	0,3708	3,254	59,377
7006	29.03.2022	0,0582	0	0,3489	3,040	52,233
7007	29.03.2022	0,0589	0	0,1921	1,600	27,168
7008	29.03.2022	0,0522	0	0,0198	0,165	3,157
7009	29.03.2022	0,0584	0	0,2810	2,398	41,068
7010	29.03.2022	0,0496	0	0,0254	0,209	4,219
7011	29.03.2022	0,0529	0	0,0123	0,105	1,992
7012	29.03.2022	0,0491	0	0,2598	2,204	44,887

Table C.13: DMA-Measurements for the blanks

Date	Absorbance cell	Peak Height	Hg (ng)	Hg Concentration(ng/g)
09.02.2022	0	0,00100	0,020	0,198
09.02.2022	0	0,00093	0,019	0,192
09.02.2022	0	0,00087	0,019	0,188
09.02.2022	0	0,00081	0,018	0,183
09.02.2022	0	0,00089	0,019	0,189
09.02.2022	0	0,00083	0,018	0,184
09.02.2022	0	0,00332	0,037	0,366
09.02.2022	0	0,00182	0,025	0,246
10.02.2022	0	0,00117	0,021	0,211
10.02.2022	0	0,00105	0,020	0,202
10.02.2022	0	0,00091	0,019	0,191
10.02.2022	0	0,00079	0,018	0,181
10.02.2022	0	0,00074	0,018	0,177
10.02.2022	0	0,00078	0,018	0,181
14.02.2022	0	0,00089	0,017	0,168
14.02.2022	0	0,00079	0,016	0,160
14.02.2022	0	0,00066	0,015	0,150
14.02.2022	0	0,00062	0,015	0,147
14.02.2022	0	0,00064	0,015	0,148
14.02.2022	0	0,00066	0,015	0,150
11.03.2022	0	0,00109	0,016	0,157
11.03.2022	0	0,00080	0,013	0,133
11.03.2022	0	0,00070	0,013	0,126
11.03.2022	0	0,00069	0,013	0,125
11.03.2022	0	0,00075	0,013	0,129
11.03.2022	0	0,00085	0,014	0,137
16.03.2022	0	0,00075	0,013	0,130
16.03.2022	0	0,00073	0,013	0,128
16.03.2022	0	0,00076	0,013	0,130
16.03.2022	0	0,00068	0,012	0,124
16.03.2022	0	0,00059	0,012	0,117
16.03.2022	0	0,00066	0,012	0,123

Date	Absorbance cell	Peak Height	Hg (ng)	Hg Concentration(ng/g)
22.03.2022	0	0,00100	0,015	0,154
22.03.2022	0	0,00096	0,015	0,150
22.03.2022	0	0,00075	0,013	0,134
22.03.2022	0	0,00083	0,014	0,140
22.03.2022	0	0,00073	0,013	0,132
22.03.2022	0	0,00074	0,013	0,134
22.03.2022	0	0,00061	0,012	0,123
29.03.2022	0	0,00089	0,017	0,172
29.03.2022	0	0,00083	0,017	0,168
29.03.2022	0	0,00077	0,016	0,163
29.03.2022	0	0,00073	0,016	0,160
29.03.2022	0	0,00063	0,015	0,152
29.03.2022	0	0,00073	0,016	0,159

Table C.14: DMA-measurements for the CRM

Date	Absorbance cell	Peak Height	Hg (ng)	Hg Concentration(ng/g)
17.01.2022	1	0,4109	9,379	135,728
17.01.2022	0	0,5832	5,521	135,328
17.01.2022	1	0,3703	8,325	142,302
18.01.2022	1	0,3056	6,663	156,030
18.01.2022	1	0,3824	8,506	133,106
18.01.2022	1	0,4407	9,968	135,797
18.01.2022	1	0,3986	8,907	133,740
18.01.2022	1	0,3444	7,584	135,190
25.01.2022	1	0,2813	6,118	129,354
01.02.2022	1	0,3001	6,553	133,725
01.02.2022	1	0,3323	7,339	141,947
01.02.2022	1	0,4482	10,368	136,247
09.02.2022	1	0,3263	7,191	133,660
09.02.2022	1	0,4609	10,724	137,311
10.02.2022	1	0,2961	6,420	141,097
10.02.2022	1	0,3415	7,515	138,916
14.02.2022	1	0,2806	6,076	128,176
14.02.2022	1	0,3178	6,966	135,781
11.03.2022	1	0,3119	6,829	131,570
11.03.2022	1	0,3452	7,640	151,893
16.03.2022	1	0,3297	7,261	133,718
16.03.2022	1	0,3333	7,350	133,872
22.03.2022	1	0,3443	7,632	152,025
22.03.2022	1	0,3350	7,404	141,037
29.03.2022	1	0,3149	6,957	137,756
29.03.2022	1	0,3574	7,980	139,030